Interface Engineering of Halide Perovskite-Based Solar Cells

M.Sc. Thesis

 $\mathbf{B}\mathbf{y}$

Juhi Gupta



DISCIPLINE OF PHYSICS INDIAN INSTITUTE OF TECHNOLOGY INDORE

 $MAY\ 2025$

Interface Engineering of Halide Perovskite-Based Solar Cells

A THESIS

Submitted in partial fulfillment of the requirements for the award of the degree

of

Master of Science

by

Juhi Gupta



DISCIPLINE OF PHYSICS INDIAN INSTITUTE OF TECHNOLOGY INDORE

 $MAY\ 2025$

CANDIDATE'S DECLARATION

I hereby certify that the work which is being presented in this thesis entitled "Interface Engineering of Halide Perovskite Based Solar Cells" in the partial fulfillment of the requirements for the award of the degree of MASTER OF SCIENCE and submitted in the DEPARTMENT OF PHYSICS, Indian Institute Of Technology Indore, is an authentic record of my own work carried out during the time period from June 2024 to May 2025 under the supervision of Dr. Onkar S. Game, Assistant Professor, Department of Physics, Indian Institute of Technology Indore.

The matter presented in this thesis has not been submitted by me for the award of any other degrees of this or any other institute.

	Juhi Gupta
This is to certify that the above statement made to the best of my knowledge.	de by the candidate is correct OSGAME 1 21 05 20 25 Dr. Onkar S. Game
	Dr. Onkar S. Game

Juhi Gupta, has successfully given her M.Sc. Oral examination held on 14/05/2025.

Supervisor Signature

Dr. Onkar S. Game Date: 21/05/2025 DPGC Signatute

Dipankan Das

Date:21/05/2025

Acknowledgment

I would like to express my heartfelt gratitude to my supervisor, Professor Onkar S. Game, Department of Physics, IIT Indore, for his constant support, invaluable guidance, and unwavering encouragement throughout the course of this project. His mentorship not only deepened my understanding of the subject but also helped me develop strong research skills.

I am sincerely thankful to Professor Rupesh S. Devan and the members of the Nano-architecture Research Group (NRG), Department of MEMS, IIT Indore, for providing laboratory facilities and extending their kind support during various phases of the project.

A special word of thanks to the Advanced Energy Materials and Devices (AEMD) research group for their enriching discussions and valuable insights, which played a significant role in shaping this work. I am particularly grateful to my lab mates Aayushi Miglani, Shyam, Aviral, and Vaibhav for their continuous help, support, and collaborative spirit, which made this journey both productive and enjoyable.

I extend my gratitude to the Department of Physics, IIT Indore, for offering me the opportunity to undertake this year-long research project. This experience has been immensely rewarding and instrumental in shaping my academic and professional growth.

I am also thankful to the Sophisticated Instrumentation Centre (SIC), IIT Indore, for providing access to advanced characterization tools, which were crucial for the experimental work carried out during the project.

My sincere thanks to my friends Chelsiya Goyal, Suman Birda, and Harshit Dubey for their constant support and encouragement throughout this journey.

Above all, I am deeply grateful to my family for their unwavering belief in me. Their love, motivation, and emotional support gave me the strength to stay focused and persevere through every challenge.

Abstract

Perovskite solar cells (PSCs) have attracted widespread attention as next-generation photovoltaic technologies due to their high power conversion efficiencies, low-cost fabrication, and solution-processable nature. However, challenges such as phase instability and defect-induced recombination continue to limit their commercial viability.

In this work, the primary goal was to stabilize the photoactive α -phase of formamidinium lead iodide (FAPbI₃), which is essential for achieving efficient and stable PSCs. To accomplish this, compositional engineering was employed—first through partial substitution with methylammonium (MA⁺), followed by the development of a triple-cation perovskite incorporating cesium (Cs⁺), resulting in the composition-

 $Cs_{0.05}FA_{0.81}MA_{0.14}PbI_{2.55}Br_{0.45}$. All devices were fabricated via a solution-based method inside a nitrogen-filled glovebox to preserve film quality.

Devices based on FA/MA compositions achieved a power conversion efficiency (PCE) of 13.33%, while triple-cation devices showed significantly improved performance, reaching a PCE of 17.46%, with enhanced J_{sc} , V_{oc} , and fill factor. To further reduce non-radiative losses and passivate interfacial defects, formamidinium acetate (FAAc), an ionic liquid, was introduced as an interface modifier. FAAc-treated devices exhibited improved V_{oc} and film uniformity, with a champion PCE of 11.15%.

This study demonstrates the effectiveness of combining compositional tuning and interfacial engineering to enhance both efficiency and stability in PSCs. The findings provide valuable insights into phase stabilization, defect passivation, and interface optimization strategies for high-performance perovskite photovoltaics.

Contents

1	Intr	roduction	1
	1.1	Historical Background of Solar Cells	1
	1.2	Generation and Types of SCs	2
	1.3	Hybrid Halide Perovskite	3
	1.4	Properties of Perovskite Material	6
		1.4.1 Absorption	6
		1.4.2 Carrier Diffusion Length	7
		1.4.3 Electronic Structure	7
	1.5	Perovskite Solar Cell (PSC)	8
	1.6	Description of the Device Layers	10
	1.7	Working Mechanism of PSCs	11
	1.8	Fundamental Challenges in PSCs	12
	1.9	Historical Efficiency Evolution of Hybrid Halide PSCs	15
2		Formamidinium Lead Iodide (FAPbI ₃) Strategies to Stabilize α -FAPbI ₃	17 17 18 18
	for 2.1 2.2 2.3	Solar Cells Formamidinium Lead Iodide (FAPbI $_3$)	17 18 18
3	for 2.1 2.2 2.3	Solar Cells Formamidinium Lead Iodide (FAPbI $_3$)	17 18
	for 2.1 2.2 2.3 Opt 3.1	Solar Cells Formamidinium Lead Iodide (FAPbI ₃) Strategies to Stabilize α-FAPbI ₃ Triple Cation Perovskite composition Simizing Interfaces in PSC Architectures FAAc as an Ionic Liquid Additive in PSCs	17 18 18 21
3	for 2.1 2.2 2.3 Opt 3.1	Solar Cells Formamidinium Lead Iodide (FAPbI ₃) Strategies to Stabilize α-FAPbI ₃ Triple Cation Perovskite composition Simizing Interfaces in PSC Architectures FAAc as an Ionic Liquid Additive in PSCs	17 18 18 21 22
3	for 2.1 2.2 2.3 Opt 3.1 Exp	Solar Cells Formamidinium Lead Iodide (FAPbI ₃) Strategies to Stabilize α-FAPbI ₃ Triple Cation Perovskite composition Simizing Interfaces in PSC Architectures FAAc as an Ionic Liquid Additive in PSCs Device Fabrication Process	17 18 18 21 22 25
3	for 2.1 2.2 2.3 Opt 3.1 Exp	Solar Cells Formamidinium Lead Iodide (FAPbI ₃) Strategies to Stabilize α-FAPbI ₃ Triple Cation Perovskite composition Simizing Interfaces in PSC Architectures FAAc as an Ionic Liquid Additive in PSCs Derimental Techniques and Procedures Device Fabrication Process 4.1.1 Preparation of the Substrate	17 18 18 21 22 25
3	for 2.1 2.2 2.3 Opt 3.1 Exp 4.1	Solar Cells Formamidinium Lead Iodide (FAPbI ₃) Strategies to Stabilize α-FAPbI ₃ Triple Cation Perovskite composition Simizing Interfaces in PSC Architectures FAAc as an Ionic Liquid Additive in PSCs Derimental Techniques and Procedures Device Fabrication Process 4.1.1 Preparation of the Substrate Device Fabrication of FAMA PSCs	17 18 18 21 22 25 25 26

5	Exp	perimental Results and Interpretation	3
	5.1	X-Ray Diffraction (XRD) : Revealing Crystal Structures	3
	5.2	UV-Vis Spectroscopy: A Tool for Bandgap Analysis	3
	5.3	Scanning Electron Microscopy (SEM):	3
	5.4	J-V Testing for Device Performance	3
		5.4.1 Solar Simulator	3
		5.4.2 J-V Measurmnet	3
	5.5	PCE Distribution Analysis	4
	5.6	Statistical Analysis of Photovoltaic Parameters	4
c		nclusion	

List of Figures

1.1	Development of SCs	2
1.2	Successive SCs Technology	3
1.3	3D schematic diagram of Perovskite (b) 2D schematic diagram of Perovskite. (c) Chemical schematic diagram of perovskite.[1]	4
1.4	Calculated tolerance Factor (t) for different A-Cite cations. [2]	5
1.5	Band edge positions and energy gaps of different halide per- ovskite compositions.[3]	6
1.6	Key features making perovskites suitable for high-performance solar cells	8
1.7	(a) mesoporous n-i-p structure, (b) conventional planar n-i-p structure, and (c) inverted planar p-i-n structure.[4]	9
1.8	Working principle of a PSC with an n-i-p architecture.[5]	11
1.9	The major challenges associated with perovskite solar cells	13
2.1	Phase transition in FAPbI ₃ : transformation between the photoactive phase (α -FAPbI ₃) and the non photoactive phase.	18
2.2	Strategies used to convert the yellow phase of FAPbI ₃ into the light-sensitive black α -phase	19
3.1	Advantages of FAAc incorporation in PSCs	23
3.2	(a) FAAc passivation at Pb and halide vacancy sites in the perovskite lattice.[6]	24
4.1	Followed Protocol for Device Fabrication	25
4.2	PSC architecture used in this study	27
4.3	Thermal vapour deposition of silver	29
4.4	Preparation Method for FAMA-Based Perovskite Solar Cells	30
4.5	Preparation Method for triple cation PSCs	32
4.6	Preparation Method for FAAc modified Perovskite Solar Cells.	32

5.1	Normalized XRD patterns of (a) FAMA and (b) Triple Cation	
	perovskite films	34
5.2	Optical bandgap determination using Tauc plots for (a) FAMA	
	and (b) triple cation perovskite films	35
5.3	(6) SEM images and (7) grain size distributions for (a) FAPbI ₃	
	and (b) triple-cation perovskite films	36
5.4	6 (a) Solar Simulator, 6 (b)) J-V curve of the FAMA PSC,	
	7 (a) J-V curve of the Triple Cation PSC, 7 (b) J-V curves	
	of the control and FAAc-modified PSCs	40
5.6	PCE distribution of control and FAAc modified perovskite	
	solar cells	41
5.8	Box plot comparison of key photovoltaic parameters for FAAc	
	modified perovskite solar cells devices	43

List of Tables

5.1	PV performance parameters of FAMA and triple cation-	
	based PSCs	39
5.2	PV parameters of control and FAAc (1%) treated devices.	39

Chapter 1

Introduction

1.1 Historical Background of Solar Cells

Among various renewable sources, solar energy is an up-and-coming option for sustainable power generation, with the potential to eventually replace conventional fossil fuels. Its environmentally friendly and pollution-free characteristics have sparked significant scientific and technological advancements in recent years [7]. Unlike fossil fuel combustion, which contributes significantly to environmental issues such as ozone layer depletion, the energy we get from the sun is a sustainable and eco-friendly. It is freely available in nature, inexhaustible, and can be harnessed efficiently through modern technology [8]. Solar cells (SCs), which form the backbone of photovoltaic (PV) technology, convert sunlight into electricity using the photovoltaic effect. The term photo relates to light, while voltaic pertains to electricity. The origin of this phenomenon dates back to 1839, when Alexandre-Edmond Becquerel observed that light could enhance the electrical output in an electrolytic cell. By the 1870s, the PV effect was further explored in solid-state materials like selenium, although early devices suffered from low efficiency and high production costs. A major breakthrough came with the introduction of the Czochralski method, which enabled the growth of high-purity silicon crystals, an essential advancement for the solar industry [9]. Today, silicon remains the most commonly used material for SCs manufacturing because of its availability, excellent electronic properties, and proven long-term stability. However, the relatively high production cost of silicon-based SCs has inspired researchers to explore alternative materials that are more cost-effective yet still deliver competitive performance. These efforts are crucial for making solar energy more accessible and for accelerating the global shift toward renewable energy solutions. The development of the SCs has been very well illustrated in Fig. 1.1

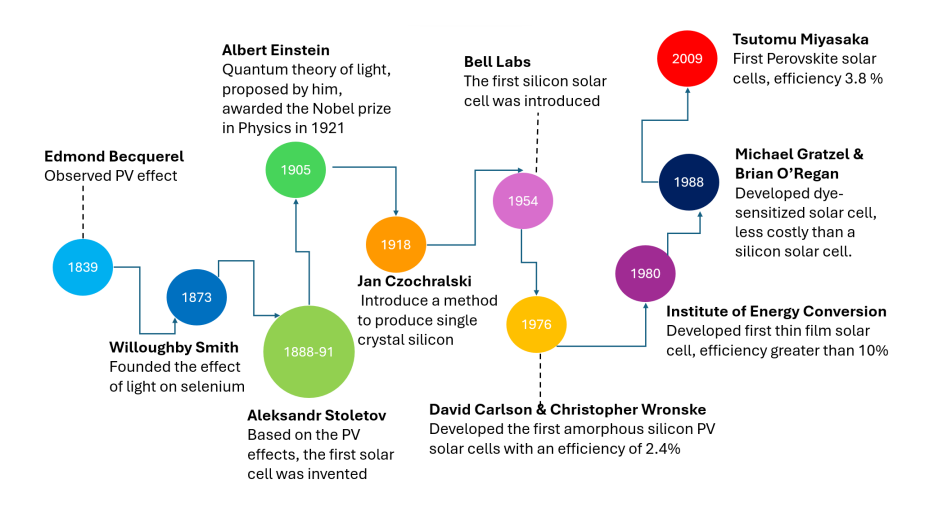


Figure 1.1: Development of SCs

1.2 Generation and Types of SCs

Based on advancements in innovation and the materials used, SCs are generally divided into three distinct generations, as illustrated in Figure 1.2.

first-generation SCs are based on wafer-based crystalline silicon technology and include monocrystalline and polycrystalline silicon cells. Monocrystalline cells offer higher efficiency but are relatively expensive, whereas polycrystalline cells are more affordable with slightly lower efficiency.

Second-generation SCs are developed using thin-film technology, allowing lightweight and flexible devices. Examples in this generation include solar cells made from CIGS, a-Si, and CdTe materials, each offering advantages in cost and material usage but often compromising on efficiency or environmental impact.

third generation (next-generation SCs), represents advanced and emerging technologies designed to overcome the limitations of earlier generations. This category comprises various types such as Technologies in this category encompass DSSCs, organic/polymer PV devices, PSCs, quantum dot SCs, and multi-junction SCs. This group focuses on achieving good efficiencies, lowering production costs, and improving flexibility.

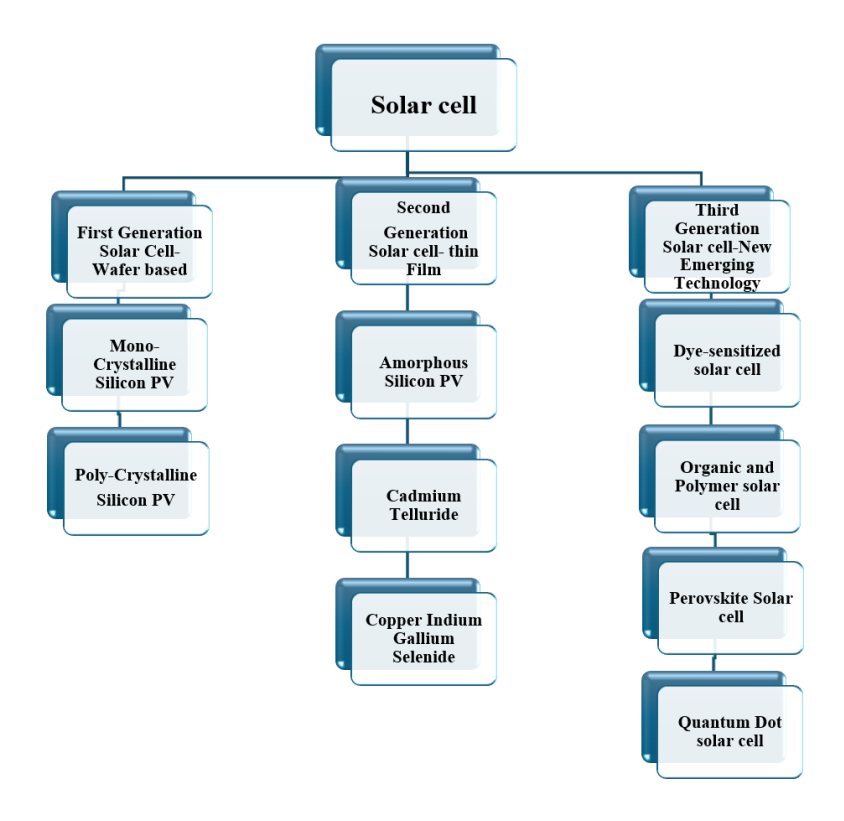


Figure 1.2: Successive SCs Technology.

1.3 Hybrid Halide Perovskite

Perovskite, a fascinating mineral first discovered in the Ural Mountains, takes its name from the unique crystal structure of calcium titanium oxide (CaTiO₃). This mineral was identified by the German mineralogist Gustav Rose in 1839 and described in detail by Russian mineralogist Lev A. Perovski, whose characterization of its distinctive cubic lattice structure laid the foundation for numerous advancements in material science and solid-state physics.

Perovskite compounds generally conform to the chemical formula ABX₃, A and B are cations of different sizes, and X is an anion—commonly a halide, oxide, or alkali element. In most cases, the A- cation is larger than the B- B-cation. The B-cation is coordinated by six X-site anions, forming a BX₆ octahedron. These octahedra are corner-sharing, creating a three-dimensional network. The larger A-site cations occupy the voids within this framework, as illustrated in Fig. 1.3.

In the ABX₃ perovskite structure, the monovalent A⁺-site cation is commonly methylammonium (MA⁺: $CH_3NH_3^+$), formamidinium (FA⁺: $HC(NH_2)_2^+$), Cs^+ , Rb^+ , or a combinations of these ions. The B²⁺ cations are usually divalent metals such as Pb^{2+} , Sn^{2+} , Ge^{2+} , or combinations of these metals. The X-site anions are typically halides as I^- , Br^- , Cl^- , or a combination of these halides [10]. These organic components introduce additional functionalities and flexibility in the structure that are not present in purely inorganic perovskites. Weber and Naturforsch first reported the incorporation of the (MA⁺) into halide perovskites in 1978, using iodide (I^-), chloride (Cl^-), and bromide (Br^-) as the halide components.[11].

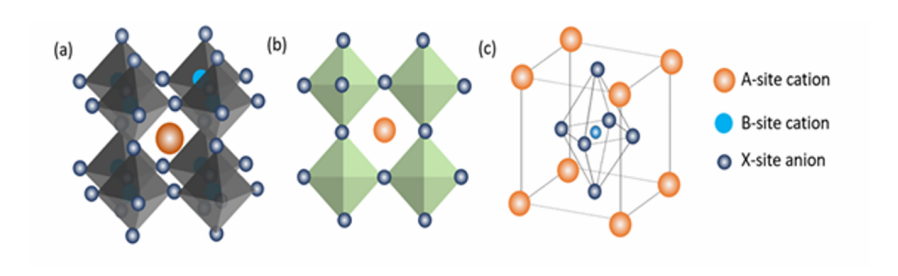


Figure 1.3: 3D schematic diagram of Perovskite (b) 2D schematic diagram of Perovskite. (c) Chemical schematic diagram of perovskite.[1]

Goldschmidt Tolerance Factor

The Goldschmidt tolerance factor (t) reflects the compatibility of ionic radii within the perovskite structure. This factor, introduced by Goldschmidt, serves as a guideline for adjusting the ionic radii about cubic symmetry, offering a method to assess the stability of the perovskite structure. [12].

$$t = \frac{R_A + R_X}{\sqrt{2}(R_B + R_X)} \tag{1.1}$$

Where R_A , R_B , and R_X indicate the ionic sizes of the A-site and B-site cations, and the X-site anion.

Cubic structures form in oxide perovskites when t is between 0.89 and 1, and in halide perovskites when t is between 0.85 and 1.11 [13]. This cubic symmetry optimizes electronic properties through strong ionic bonding.

Deviations from the ideal tolerance range cause octahedral tilting, negatively affecting these properties. When t < 1, B-X bonds compress while A-X bonds become tense to fill voids, leading to reduced symmetry. Conversely, when t > 1, typically due to smaller B-site cations or larger A-site,

the structure gains higher symmetry and stability, often adopting a hexagonal arrangement.

Additionally, the dimensionality of perovskites varies based on the sizes of their components as shown in Fig. 1.4

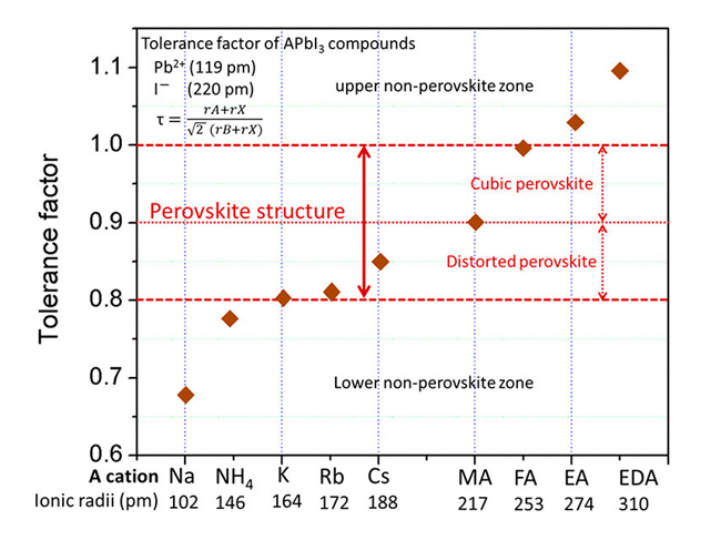


Figure 1.4: Calculated tolerance Factor (t) for different A-Cite cations. [2]

Octahedral Factor

Li and co-workers proposed the octahedral factor (μ) [14], which quantifies the ratio between the ionic radius of the B-site cation and that of the X-site anion, and is expressed as follows:

Octahedral factor
$$(\mu) = \frac{R_B}{R_X}$$
 (1.2)

 (μ) is directly related to the stability of the (BX_6) octahedron. Halide perovskite formation is generally possible when $\mu > 0.442$. If the octahedral factor falls below this threshold, the (BX_6) octahedron becomes unstable, thereby preventing the formation of a stable perovskite structure.

While (μ) , in conjunction with the tolerance factor, provides a useful guideline for assessing the formability of halide perovskites, these parameters alone are not sufficient to predict all structural formations of the perovskite family [15].

1.4 Properties of Perovskite Material

1.4.1 Absorption

Hybrid perovskites are known for their outstanding optical absorption capabilities, which enable the use of much thinner active layers in solar cells compared to traditional materials. A perovskite film as thin as 500 nm can efficiently absorb light across the entire visible spectrum, whereas conventional solar cell materials typically require active layers around 2 μ m thick to achieve similar absorption. This ultra-thin profile not only reduces material usage but also enhances charge carrier collection efficiency.

Recent advancements have demonstrated that mixed-cation perovskites, such as $MASn_xPb_{1-x}I_3$, can extend the absorption edge significantly. As the tin content (x) increases from 0.3 to 1.0, the absorption edge shifts from 1000 nm to 1300 nm, effectively moving into the near-infrared region. This shift is attributed to changes in the electronic band structure: the valence band lowers from 5.12 eV to 4.73 eV, while the conduction band rises from 3.18 eV to 3.63 eV.

Additionally, perovskites based on formamidinium lead iodide (FAPbI₃) exhibit reduced band gaps of around 1.48 eV, with absorption onsets near 850 nm. Further band gap tuning can be achieved by partially substituting iodide with bromide in the composition FAPbI_{3-x}Br_x, enabling precise control over optical properties to match specific device requirements.

These trends are clearly illustrated in Figure 1.5, which compares the band edge positions and energy gaps of various halide perovskite compositions, highlighting their tunability and potential for high-efficiency photovoltaic applications.

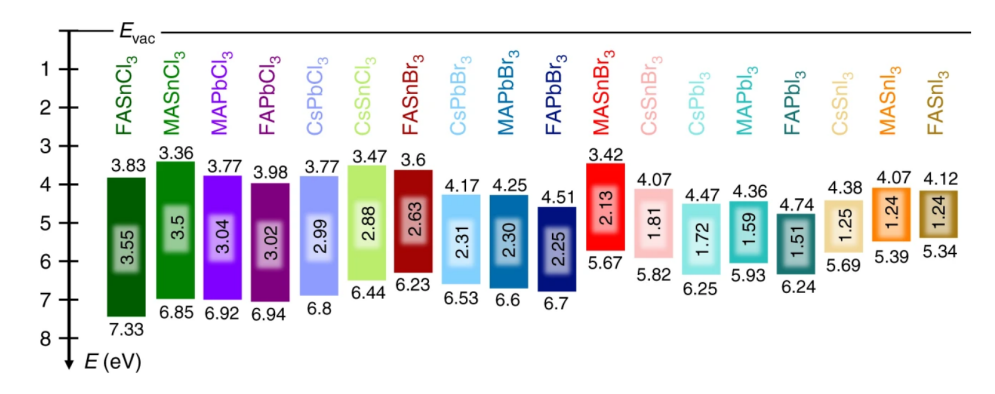


Figure 1.5: Band edge positions and energy gaps of different halide perovskite compositions.[3]

1.4.2 Carrier Diffusion Length

Carrier diffusion length is a key parameter that influences charge collection efficiency in photovoltaic materials. In methylammonium lead iodide (MAPbI₃), diffusion lengths of up to 100 nm for both electrons and holes have been observed using transient photoluminescence (PL) techniques.[16] However, significantly longer diffusion lengths exceeding 1 μ m have been reported in mixed halide perovskites such as MAPbI_{3-x}Cl_x, indicating improved charge transport properties.

More notably, Dong et al. demonstrated that single crystals of MAPbI₃ exhibit carrier diffusion lengths beyond 175 μ m under standard 1 sun illumination. This substantial enhancement is attributed to several factors: higher carrier mobility, extended carrier lifetimes, and a lower density of trap states within the crystalline lattice.[17] These improvements showing the potential of high-quality perovskite single crystals for achieving the stable solar cells, as they enable more effective charge extraction and reduce recombination losses.

1.4.3 Electronic Structure

Extensive research into the electronic structures of both two-dimensional (2D) and three-dimensional (3D) hybrid perovskites has revealed that their band edges are primarily governed by interactions within the inorganic framework. Specifically, the valence band maximum (VBM) originates from an antibonding hybrid state formed between the B-site metal s-orbitals and the halide p-orbitals (B–s and X–p). In contrast, the conduction band minimum (CBM) arises from a non-bonding interaction involving the B-site p-orbitals and the halide p-orbitals (B–p and X–p).

First-principles pseudopotential calculations conducted by Park and Chang in 2004 examined the electronic properties of MAPbI $_3$ and CsPbX $_3$ systems. Their findings indicated that the electronic levels associated with the organic methylammonium (MA) cation lie deep in the VB and CB, contributing minimally to the electronic properties near the band edges. As a result, the frontier electronic states are primarily determined by the BX $_6$ octahedra.

This also explains why the substitution of the A site from organic (MA⁺) to inorganic (Cs⁺) has only a minor influence on the band structure, mainly due to lattice distortion effects. However, changes in the halide composition significantly affect the electronic states, allowing for band gap tuning.

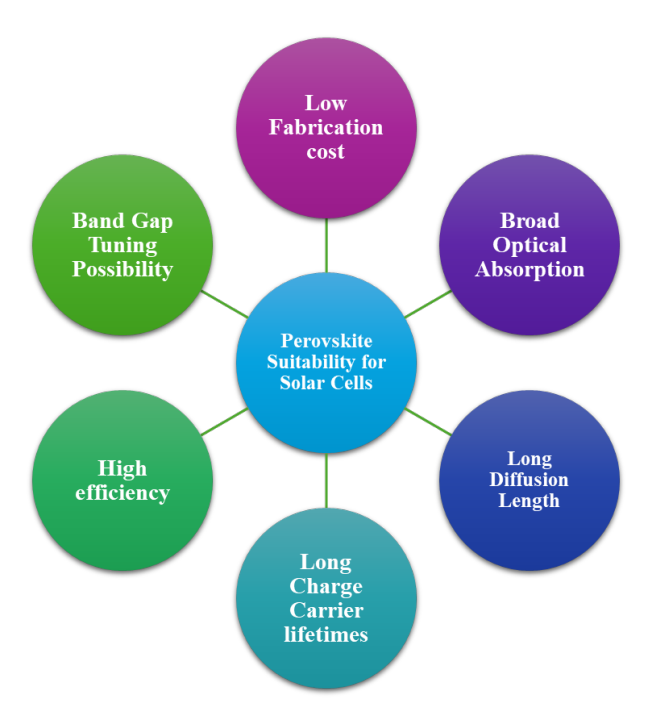


Figure 1.6: Key features making perovskites suitable for high-performance solar cells.

1.5 Perovskite Solar Cell (PSC)

The journey of hybrid perovskites in solar technology began in 2006, when Miyasaka and his team introduced CH₃NH₃PbBr₃ as a light-absorbing material in (DSSCs). Utilizing a nanoporous TiO₂ layer and a liquid electrolyte, this early device gained a modest power conversion efficiency of 2.2%. Despite the humble beginning, this milestone sparked a wave of research interest in organic-inorganic hybrid halide perovskites. Since that time, significant progress in material engineering and device structures has greatly enhanced the efficiency and stability of PSC, positioning them as a strong contender for future energy applications.

Types of PSC

PSCs are classified into various types depending on their composition and structure. According to the architecture, they can be grouped into three main categories.

1. Mesoporous PSC In this configuration, fig. 1.7 (c), the device typically begins with FTO. A compact layer of titanium dioxide (TiO_2), approximately 80 nm thick, is deposited on top to function as the (ETL). Above this, a mesoporous TiO_2 scaffold—around 350 nm in thickness—is

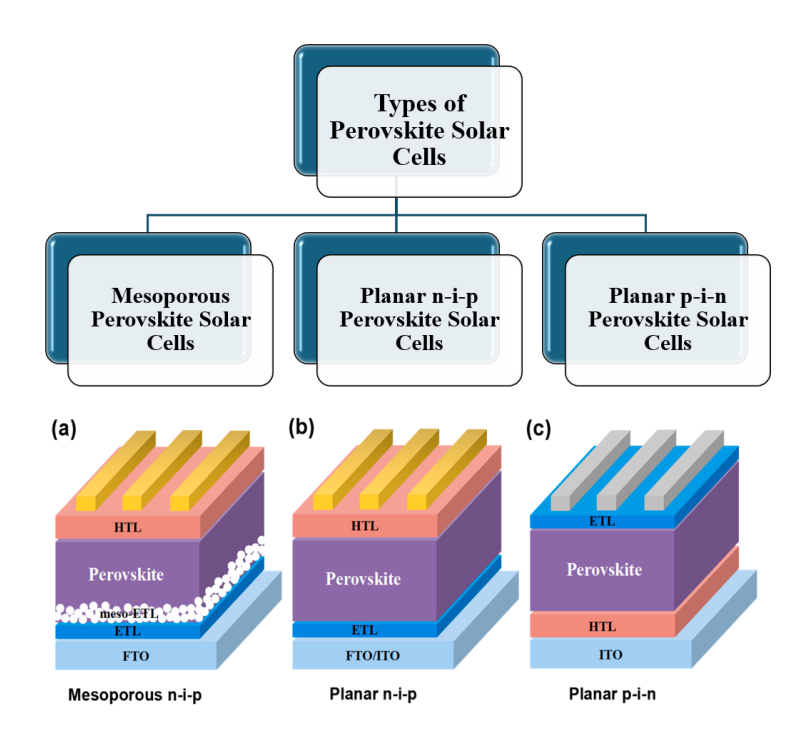


Figure 1.7: (a) mesoporous n-i-p structure, (b) conventional planar n-i-p structure, and (c) inverted planar p-i-n structure.[4]

applied to provide structural support and facilitate the infiltration of the perovskite absorber material. Once the perovskite is incorporated into the scaffold, a (HTL) is added, commonly using the organic semiconductor spiro-OMeTAD. Finally, the device is completed with the deposition of a gold layer, about 100 nm thick, which acts as the top electrode. This layered design enables efficient charge separation and collection, contributing to the high performance of mesoporous PSCs .[18]

- **2. Planar n-i-p PSC** A common *n-i-p* structure consists of the following layers in order: TCO/ETL/Perovskite/HTL/Metal. In this arrangement, the ETL is applied first, followed by the perovskite absorber, and finally the HTL.
- **3. Planar p-i-n PSC** Conversely, the *p-i-n* configuration represents an inverted structure, and its layer order is: Glass/TCO/HTL/Perovskite/ETL/metal. In this structure, the HTL is deposited first.

Figure 1.7 explains the complete device structure, including the mesoporous architecture and layer sequences of both n-i-p and p-i-n configurations.

1.6 Description of the Device Layers

1. Transparent Conductive Oxides (TCOs): TCOs are essential components in PSCs, functioning as the front electrode. They enable light to enter the device while also conducting the charge carriers generated during operation. Commonly used TCOs are fluorine-doped tin oxide (FTO) and indium tin oxide (ITO). FTO is preferred for its thermal stability and compatibility with high-temperature processes, while ITO offers better transparency and lower resistivity but is more expensive and less thermally stable.

TCOs form the base layer on which the rest of the device structure is built. They must have high optical transmittance, low electrical resistance, and good chemical and mechanical stability. Although alternative materials like aluminum-doped zinc oxide (AZO) are being explored, FTO and ITO remain the most widely used in both research and early-stage commercial devices.

2. Electron Transport Layer (ETL): ETLs are essential in PSCs as they facilitate the effective collection and movement of photo-generated electrons. Besides their primary role in electron collection, ETLs also act as hole-blocking layers, effectively minimizing charge recombination at the interface and thereby increasing the overall PCE of the device.

Inorganic and organic materials have been utilized as ETLs in PSCs. Common inorganic ETLs include titanium dioxide (TiO_2) , zinc oxide (ZnO), and tin oxide (SnO_2) , while organic ETLs primarily consist of materials like phenyl-C61-butyric acid methyl ester (PCBM) and C60.

Among these, SnO₂ has gained particular attention in n-i-p structured devices due to its excellent electron mobility, high optical transparency, low-temperature processability, and long-term operational stability. These features make it a highly promising candidate for scalable and efficient PSC. [19]

- 3.Perovskite Layer: The perovskite layer, typically composed of organic-inorganic metal halide compounds with the formula ABX₃ (e.g., MAPbI₃, FAPbI₃, etc.), serves as the light-absorbing material in PSCs. Because of its direct band gap, high absorption coefficient, long carrier diffusion lengths, and tunable optoelectronic properties, this layer plays an important role in efficient photon harvesting and charge carrier generation. Its solution-processability and compatibility with low-temperature fabrication further enable cost-effective and scalable device production.
- 4. Hole Trasport Layer (HTL): HTL is essential for efficiently extracting and transporting photogenerated holes from the perovskite's pho-

toactive layer to the top electrode in PSCs. Choosing the right HTL material depends on factors like hole mobility, stability, HOMO level alignment, and compatibility with the device fabrication process.

In 2012, spiropyridine-OMeTAD (spiro-OMeTAD) was introduced as the first HTM in all-solid-state PSCs and remains the most widely used due to its effective hole transport properties. However, its performance often requires additives like 4-tert-butylpyridine (tBP) and Li-TFSI to improve conductivity and stability.

Although spiro-OMeTAD remains dominant, ongoing research is exploring alternative HTMs to enhance stability, reduce costs, and improve scalability for commercial applications.[20]

5.Charge Collection Electrode: In PSCs, gold is used as the top electrode due to its high conductivity and stability. However, its high cost is a drawback, making silver a more economical alternative, as it is approximately 65 times cheaper. The major issue with silver electrodes is corrosion, which occurs when silver forms silver halides upon contact with perovskite material. This corrosion typically begins within days of fabrication, leading to discoloration and a decrease in device efficiency.

Research is ongoing to address silver corrosion, with efforts exploring corrosion-resistant alloys or alternative materials like copper and carbon, along with encapsulation techniques to improve device stability.

1.7 Working Mechanism of PSCs

The operation of a PV cell involves several key steps, as illustrated in Figure 1.8, which can be summarized as follows:

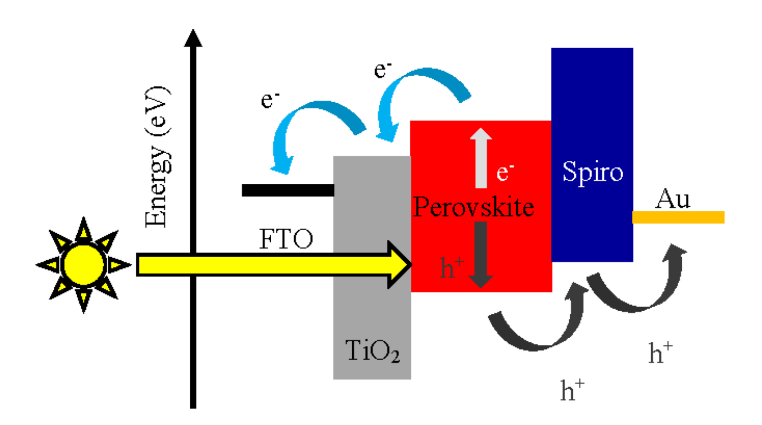


Figure 1.8: Working principle of a PSC with an n-i-p architecture. [5]

- 1. Absorption of Photons: When sunlight irradiates the SCs surface, photons are absorbed by the active layer, typically composed of a perovskite semiconductor. This photon absorption excites electrons from the VB to the CB, resulting in the generation of excitons, which subsequently dissociate into free charge carriers under thermal energy or internal electric fields.
- 2. Seperation of charges: Efficient charge separation is facilitated by the energy level alignment of the adjacent charge transport layers:ETL and HTL. ETL selectively extracts electrons from the perovskite layer and blocks holes, while the HTL performs the inverse function. This band alignment creates a built-in electric field that drives the spatial separation of electrons and holes, significantly suppressing recombination losses and enhancing charge extraction efficiency.
- **3. Collection of Charges:** The free carriers are then transported to the respective electrodes via the ETL and HTL. TCOs (e.g., indium tin oxide) or metallic contacts (e.g., silver or gold) are employed as electrodes, enabling efficient collection of electrons and holes. These electrodes establish electrical contact with the external circuit.
- 4. Current Generation: Under illumination, photogenerated electrons and holes are transported through their respective selective layerselectrons via the ETL and holes via the HTL toward the cathode and anode, respectively. When an external electrical load is connected across the electrodes, a closed-loop circuit is established. The separated charge carriers are then driven through the external circuit due to the built-in potential difference across the device, resulting in the generation of a direct current (DC). [21]

1.8 Fundamental Challenges in PSCs

PSCs have gained significant attention as a leading PV technology because of their outstanding PCE, low-cost fabrication processes, and tunable optoelectronic properties. However, despite the rapid progress in laboratory-scale devices, several critical challenges hinder their commercial viability and large-scale deployment. These issues can be broadly categorized into the following areas: fig. 1.9

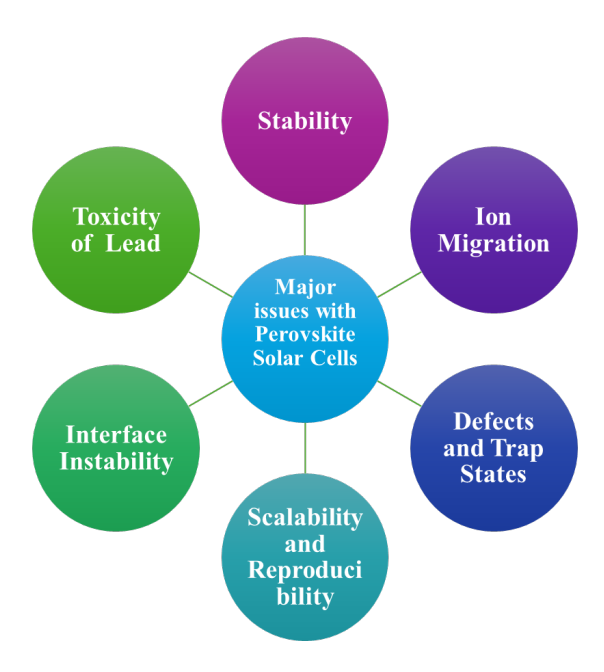


Figure 1.9: The major challenges associated with perovskite solar cells.

Stability

Perovskite materials are very sensitive to external factors such as moisture, oxygen, ultraviolet radiation, and heat. Exposure to these conditions can lead to rapid degradation of the perovskite layer, resulting in significant performance losses over time. The intrinsic thermal and chemical instability of some perovskite compositions, such as pure FAPbI₃, also contributes to phase transitions from the photoactive phase to a non-photoactive phase under ambient conditions. [3]

Ion Migration

The flexible ionic structure of perovskite materials enables ion migration within the lattice. (e.g., I⁻, MA⁺, FA⁺) within the lattice under the influence of an electric field or illumination. This ion migration can cause current–voltage hysteresis, affect device reproducibility, and contribute to long-term performance instability. Additionally, mobile ions can accumulate at interfaces and degrade the transport layers or electrodes.[3]

Defects and Trap States

Perovskite thin films often contain structural imperfections such as grain boundaries, surface defects, and undercoordinated ions. These defects serve as the centers for non-radiative recombination, limiting charge carrier lifetimes and reducing open-circuit voltage. Defect passivation remains a major research focus to improve the stability of PSCs.[22]

Scalability and Reproducibility

Although high efficiencies have been gained in small-area devices, scaling up PSCs to large-area modules while maintaining uniform film quality and device performance remains challenging. Variations in precursor solution chemistry, film crystallization kinetics, and interface engineering strategies can lead to inconsistent results across different fabrication batches and laboratories. [23]

Toxicity of Lead

The PSCs are based on lead halide compounds, which raise environmental and health concerns. While the total amount of lead in a single device is relatively small, the risk of lead leakage during degradation or disposal poses a potential hazard. Research is ongoing to develop lead-free or lead-reduced alternatives, but these materials currently suffer from lower efficiencies and reduced stability. [24]

Interface Instability

Interfacial regions connecting the perovskite layer with the charge extraction layers are often chemically reactive or structurally mismatched. Degradation can occur due to interdiffusion, unfavorable reactions, or the formation of energy barriers, all of which hinder efficient charge extraction and reduce device lifetime. Proper interface engineering is essential to overcome these issues. [25]

In summary, while PSCs are great for next-generation PV, overcoming their stability, toxicity, and scalability challenges is essential for transitioning from laboratory prototypes to commercially viable products. Addressing these issues requires a holistic approach involving material design, device architecture optimization, and advanced encapsulation strategies.

1.9 Historical Efficiency Evolution of Hybrid Halide PSCs

The development of hybrid halide PSCs has redefined the landscape of photovoltaic research due to their exceptional and rapid rise in PCE. Over a span of just 15 years, PSCs have progressed from laboratory curiosities to serious contenders in the commercial solar energy market. This section outlines the major efficiency milestones in the evolution of PSCs, highlighting the underlying breakthroughs that enabled this growth.

2009 – Initial Demonstrations

Kojima et al. first introduced PSCs in 2009, reporting a PCE of 3.8%. They employed MAPbX₃, where X = Cl, Br, or I, as the light-absorbing material within a DSSC configuration using a liquid electrolyte. While the efficiency was modest, the study was significant for showcasing the strong light absorption capabilities of perovskite materials and their potential as photovoltaic absorbers.

2012–2015 – Rapid Optimization and Transition to Solid-State Devices

A key breakthrough occurred in 2012 when perovskites were incorporated into solid-state architectures using hole transport materials like spiro-OMeTAD and inorganic metal oxides such as TiO_2 . The elimination of liquid electrolytes significantly improved device stability and allowed researchers to explore film deposition techniques, leading to better morphology and interface quality. During this period, PCEs quickly rose from $^{\sim}9\%$ to over 19%, driven by advances such as improved control over perovskite crystallization, the introduction of mixed halide systems (e.g., MAPbI_{3-x}Cl_x), and the use of mesoscopic scaffolds to enhance charge extraction. [26]

2015–2018 – Technological Maturity and Compositional Engineering

This period marked the transition from methylammonium (MA)-based perovskites to more thermally and structurally stable formulations using formamidinium (FA), cesium (Cs), and mixed-cation/anion compositions. For example, triple-cation perovskites (FA_xMA_yCs_{1-x-y}PbI_{3-z}Br_z) provided enhanced thermal stability, reduced trap densities, and better phase purity, which collectively contributed to more consistent and higher efficiencies. Researchers also began focusing on interface engineering, defect passivation, and optimization of transport layers, pushing device efficiencies above 20%.[27]

2018–2025 – State-of-the-Art Devices and Record Efficiencies

By 2018, certified PCEs surpassed 23%, and further refinement in materials chemistry and device architecture led to the development of record-breaking devices. As of 2025, the efficiency of single-junction PSCs has reached 26.1%, rivaling established technologies like monocrystalline silicon. This progress is attributed to precise control over perovskite film quality, improved charge carrier mobility, minimized non-radiative recombination, and the adoption of scalable fabrication techniques. Additionally, the emergence of tandem solar cells—especially perovskite/silicon tandems—has opened a new frontier, with efficiencies exceeding 33%, signaling the potential of perovskites in breaking the limitations of single-junction devices.

In summary, the efficiency progression of hybrid halide PSCs from 3.8% to 26.1% within approximately 15 years is unprecedented in photovoltaic research. Each stage of this evolution reflects significant material and engineering innovations, including the shift from liquid to solid-state architectures, compositional tuning, crystallization control, and defect mitigation.

Chapter 2

Compositional Variations of Halide Perovskite Materials for Solar Cells

2.1 Formamidinium Lead Iodide (FAPbI₃)

FAPbI₃ exhibits two main phases: a cubic perovskite structure, which appears black and is stable only at temperatures above 150°C, and a yellow-colored, non-perovskite hexagonal phase that is more stable at room temperature [?], as shown in Fig. 2.1. The black perovskite phase, referred to as α -FAPbI₃, is particularly advantageous for PSCs due to its band gap of 1.48 eV. This value closely matches the ideal band gap of 1.4 eV predicted by the Shockley–Queisser limit, enabling the material to achieve power conversion efficiencies exceeding 32% [28].

Compared to MAPbI₃, the α -FAPbI₃ phase offers superior thermal stability [29], making it a strong candidate for photovoltaic applications. However, maintaining its photoactive black phase at room temperature is challenging, as it tends to revert to the non-photoactive yellow phase. Achieving a stable α -FAPbI₃ film often requires high processing temperatures, which may lead to partial decomposition into PbI₂.

The structural stability of FAPbI₃ is largely influenced by entropy, which is linked to the dynamic behavior of FA⁺ (formamidinium) cations. At elevated temperatures, these cations exhibit random motion, resulting in high configurational entropy that stabilizes the cubic α -phase.

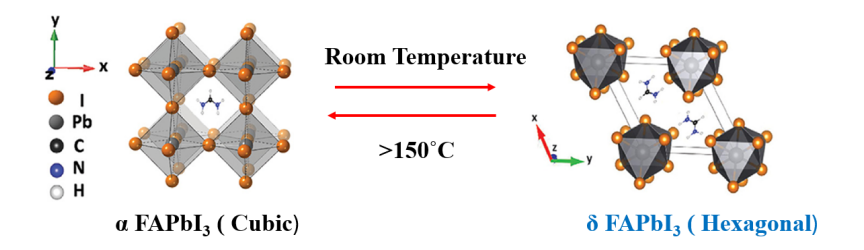


Figure 2.1: Phase transition in FAPbI₃: transformation between the photoactive phase (α -FAPbI₃) and the non photoactive phase.

2.2 Strategies to Stabilize α -FAPbI₃

The conversion from the yellow non photoactive phase to the photoactive black α -phase in FAPbI₃ is difficult because it involves overcoming a high energy barrier. This challenge makes it hard to obtain a pure and stable black photoactive perovskite phase under ambient conditions.

However, several strategies have been proposed to reduce this energy barrier and stabilize the photoactive α -phase as shown in fig. 2.2 Researchers have explored a variety of approaches to achieve the formation of the black phase, including:

- Manipulation of the Intermediate Phase: Controlling the intermediate phase during film formation can guide the transition toward the desired black perovskite structure.
- Strain Engineering: Applying lattice strain through substrate interaction or material additives can energetically favor the formation of the α -phase.
- Two-Step Solution Process: Sequential deposition techniques, such as a two-step solution method, have proven effective in promoting the phase transition with enhanced film uniformity and crystallinity.

These techniques are instrumental in overcoming the thermodynamic limitations associated with the phase transition.

2.3 Triple Cation Perovskite composition

Compositional engineering is a well-established method to stabilize the photoactive black α -phase of FAPbI₃.Research suggests that incorporating

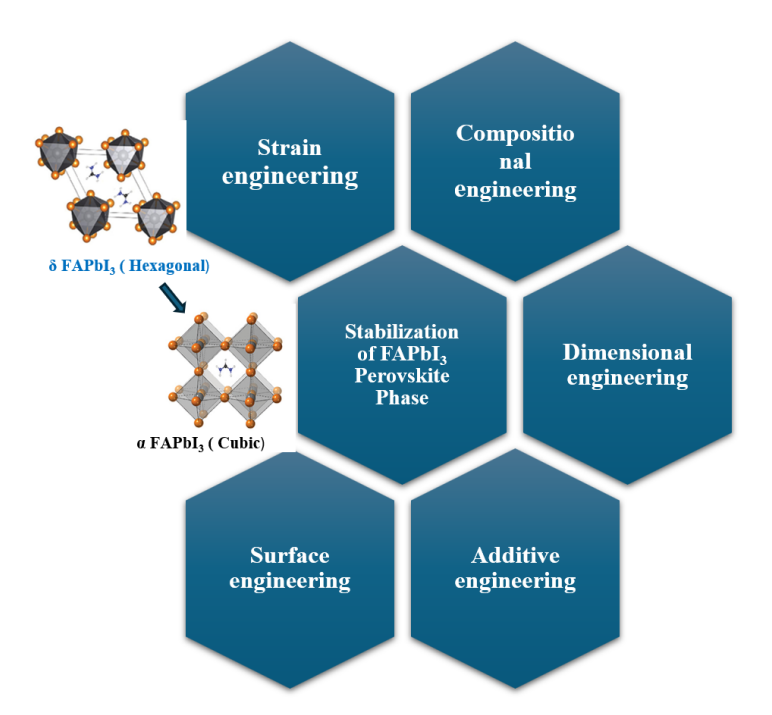


Figure 2.2: Strategies used to convert the yellow phase of FAPbI₃ into the light-sensitive black α -phase.

monovalent cations such as MA⁺, Rb⁺, and Cs⁺, or halide anions like Br⁻, can help maintain the structural and thermal stability of the perovskite lattice [30].

Partial substitution of the formamidinium $(FA^+ \text{ or } HC(NH_2)_2^+)$ cation with Cs^+ in the range of 5–10% has been shown to significantly improve the humidity resistance and photostability of perovskite layers. One key reason for this stabilization is that the incorporation of Cs^+ lowers the Goldschmidt tolerance factor [31], leading to enhanced lattice stability and phase retention.

Incorporating 15% MAPbBr₃ into FAPbI₃ forms a more stable perovskite composition, namely (FAPbI₃)_{0.85}(MAPbBr₃)_{0.15}. This ternary structure benefits from the strong dipole moment of MA⁺ approximately ten times stronger than that of FA⁺ which enhances the rigidity of the PbI₆ octahedral network [32]. Furthermore, Br⁻ anions form stronger bonds with the surrounding lattice compared to I⁻, providing additional structural reinforcement and improved phase stability.

Given these benefits, a triple-cation perovskite composition was selected for this study. Experimental fabrication of stacked n-i-p structured SCs was

carried out in a controlled glovebox environment to prevent moisture and oxygen exposure. This approach was employed to simultaneously enhance both device stability and efficiency while ensuring a reproducible and optimized fabrication process.

Chapter 3

Optimizing Interfaces in PSC Architectures

In PSCs, the interfaces between different functional layers play a very important role in determining the overall performance, stability, and reproducibility of the device. These interfaces include the junctions between the perovskite absorber layer and the charge transport layers, as well as the interfaces with electrodes. Imperfections at these interfaces, such as trap states, energy level mismatches, poor adhesion, or chemical incompatibilities, can lead to increased recombination losses, reduced charge extraction efficiency, and degraded device stability.

Interface modification refers to the strategic engineering of these interfacial regions to overcome such limitations and to increase the performance of PSCs. This can involve the introduction of interfacial layers, surface passivation agents, molecular additives, ionic liquids, or two-dimensional materials that improve the electronic properties of the interface.

The goals of interface modification include:

- Defect passivation: Reducing trap states and recombination centers that exist at grain boundaries or surfaces.
- Energy level alignment: Tailoring energy band alignment to facilitate efficient charge extraction and reduce energy losses.
- Enhancing stability: Preventing ion migration and improving resistance to moisture and thermal stress.
- Improving morphology: Promoting uniform perovskite film growth with better coverage and fewer pinholes.

In this thesis, interface modification was explored as a method to passivate defects and enhance the stability and performance of the fabricated PSCs. By adding a small amount of the ionic liquid formamidine acetate (FAAc) into the PbI₂ precursor, changes at the interface were induced that contributed to improved open-circuit voltage and device behavior. This approach highlights the importance of precise interfacial control in achieving high-efficiency and stable PSCs.

3.1 FAAc as an Ionic Liquid Additive in PSCs

The incorporation of formamidine acetate (FAAc) into the PbI₂ precursor solution plays a multifaceted role in enhancing the performance of PSCs, primarily through defect passivation, crystal quality improvement, and interface modulation.

FAAc contains formamidinium (FA⁺) cations and acetate (CH₃COO⁻) anions. Upon addition to the PbI₂ precursor, the FA⁺ ions contribute to the perovskite lattice formation, while the acetate ions interact with undercoordinated Pb²⁺ ions at the surface and grain boundaries. This interaction can reduce non-radiative recombination centers, which are often associated with iodide vacancies or undercoordinated lead atoms, by passivating surface and interfacial defects.

The strong interaction between acetate anions and Pb²⁺ ions leads to the formation of intermediate phases, which play a key role in controlling the perovskite crystallization dynamics.

These intermediates can regulate the nucleation and growth kinetics of the perovskite film, leading to larger grain sizes, reduced grain boundary density, and improved film uniformity. As a result, the perovskite layer exhibits fewer charge-trapping sites and better carrier transport pathways.

Furthermore, the FA⁺ cations help in stabilizing the photoactive black-phase (α -phase) of formamidinium lead iodide (FAPbI₃), which is thermodynamically unstable in its pure form under ambient conditions. The presence of FA⁺ from FAAc supplementation enhances the compositional balance and supports the retention of the α -phase, contributing to long-term device stability.

Experimentally, the inclusion of 1 mol% FAAc in the PbI₂ precursor was found to enhance the (V_{OC}) , which is a clear indicator of reduced non-radiative recombination losses. Although a reduction in J_{SC} and FF was observed in this specific configuration, the increase in V_{OC} confirms the defect passivation role of FAAc. In summary, FAAc improves the quality of the perovskite layer both structurally and electronically. Its dual role

acting as a passivating agent and stabilizer, contributes to enhanced charge carrier dynamics and improved photovoltaic performance. These findings underline the significance of interfacial chemical engineering in optimizing the performance and reliability of PSCs [6]

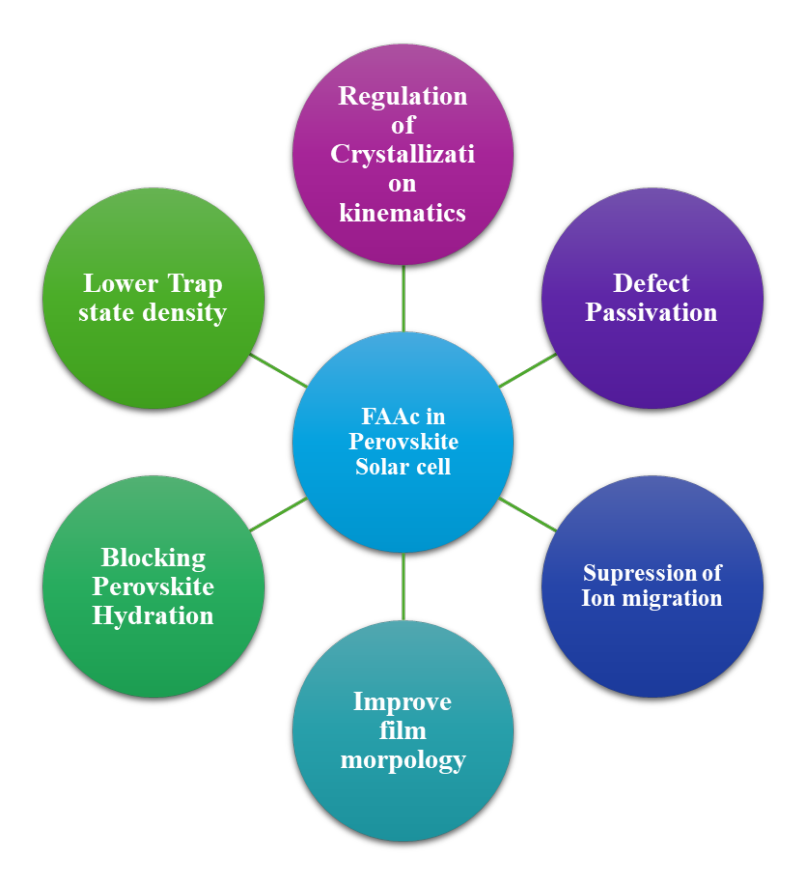


Figure 3.1: Advantages of FAAc incorporation in PSCs.

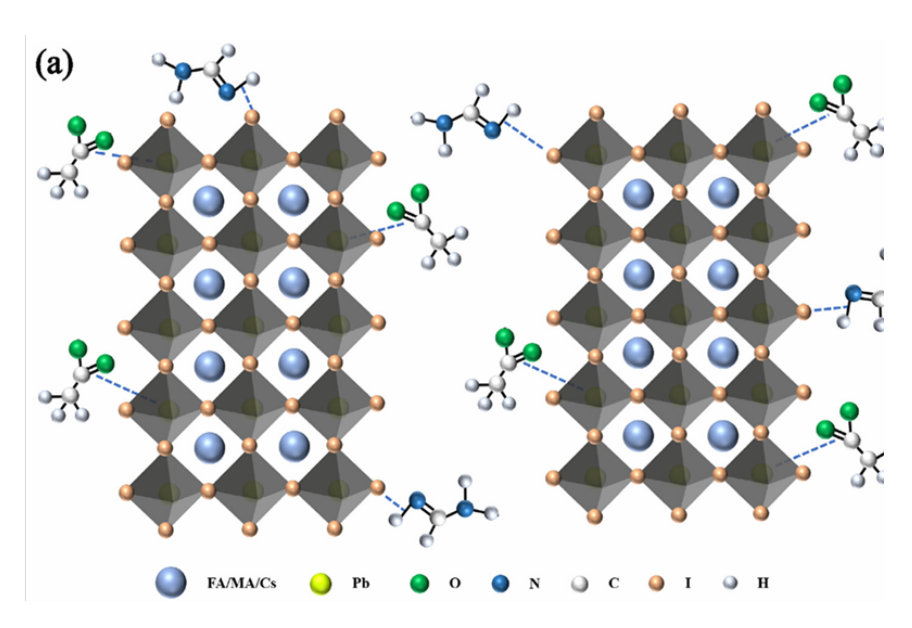


Figure 3.2: (a) FAAc passivation at Pb and halide vacancy sites in the perovskite lattice. [6]

Chapter 4

Experimental Techniques and Procedures

4.1 Device Fabrication Process

Perovskite materials have shown the ability to perform all the essential roles needed for photovoltaic (PV) operation. As a result, planar configurations have become a key design choice for these materials. In our device fabrication, we are focusing on the planar n-i-p perovskite structure. Fig. 4.1 shows the complete device fabrication Process.

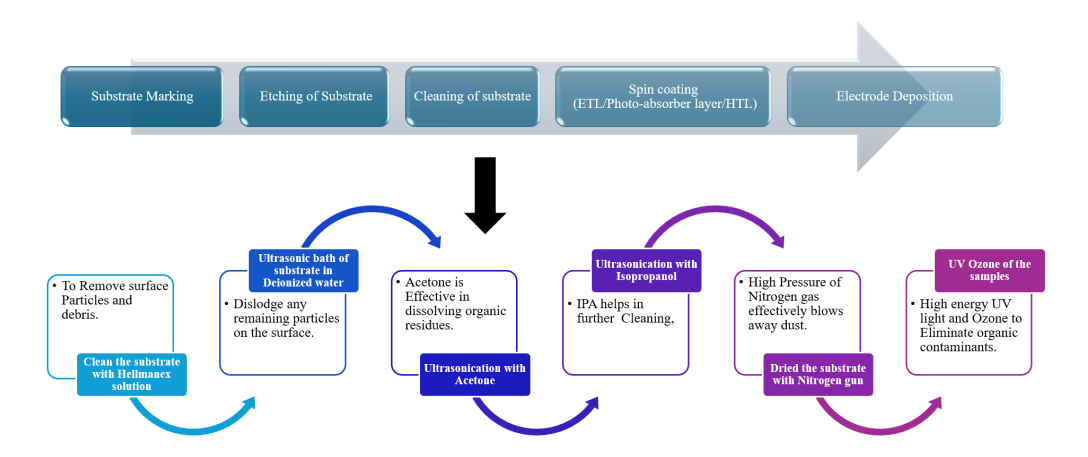


Figure 4.1: Followed Protocol for Device Fabrication

4.1.1 Preparation of the Substrate

Substrate Cleaning Procedure: In the standard n-i-p device architecture, ITO serve as the transparent conductive electrode. Cleaning the ITO substrate is a fundamental and essential step in the fabrication of PSCs. Even minute surface contaminants can adversely affect film uniformity, layer adhesion, and overall device efficiency.

The ITO substrates, typically cut to dimensions of $2 \text{ cm} \times 1.5 \text{ cm}$, undergo a rigorous cleaning process to ensure a pristine surface for subsequent layer deposition [33]. The cleaning protocol consists of the following steps:

- 1. Scrub the substrates thoroughly with a Hellmanex cleaning solution, taking care to avoid surface scratches or damage to the ITO layer.
- 2. Rinse the substrates extensively with deionized (DI) water to remove any residual detergent.
- 3. Place the substrates in an ultrasonic bath filled with DI water and sonicate for approximately 15 minutes.
- 4. Transfer the substrates to a second ultrasonic bath containing isopropanol (IPA) and sonicate for another 15 minutes.
- 5. Rinse thoroughly with fresh IPA to eliminate any remaining impurities.
- 6. Rapidly dry the substrates using a strong flow of nitrogen gas.
- 7. Expose the substrates to UV-ozone treatment for 30 minutes. This step increases the hydrophilicity of the surface, enhancing wettability and promoting uniform film formation, which is critical for achieving high-efficiency PSCs.

It is essential to proceed with the deposition steps immediately after the cleaning process to prevent recontamination of the substrate surface.

Etching Mechanism: Precise patterning of the ITO layer is essential for the fabrication of PSCs. Selective removal of the ITO layer is achieved by masking designated regions using Kapton tape, followed by a chemical etching process. The etching involves applying zinc powder and 3M hydrochloric acid (HCl) solution onto the unmasked areas.

• Chemical Reaction: Zinc reacts with hydrochloric acid to produce nascent hydrogen (H₂) and zinc chloride (ZnCl₂), as shown in Equation 4.1.

$$\operatorname{Zn}(s) + 2\operatorname{HCl}(\operatorname{aq}) \to \operatorname{ZnCl}_2(\operatorname{aq}) + \operatorname{H}_2(g)$$
 (4.1)

• Reduction of ITO: The nascent hydrogen acts as a reducing agent, breaking down the indium oxide (In₂O₃) and tin oxide (SnO₂) components of ITO into their metallic or soluble forms, as illustrated in Equation 4.2.

$$In_2O_3 + 6H_2 \rightarrow 2In + 3H_2O$$
 (4.2)

After etching, the exposed regions are carefully cleaned using a cotton swab, followed by thorough rinsing with deionized (DI) water to remove any residual etchants or by-products. This patterning process is critical to achieving efficient device architecture, enabling accurate electrical isolation and optimized performance of PSCs.

Layers Deposition The fabrication process of PSCs involves spin-coating multiple functional layers, each playing a vital role in the device performance. The PSC fabricated in this study adopts the following n-i-p architecture: ITO / ETL (SnO₂) / Perovskite / HTL (Spiro-OMeTAD) / Ag. This structure is also depicted schematically in Fig. 4.2, showing the layer-by-layer configuration essential for efficient charge transport and extraction.

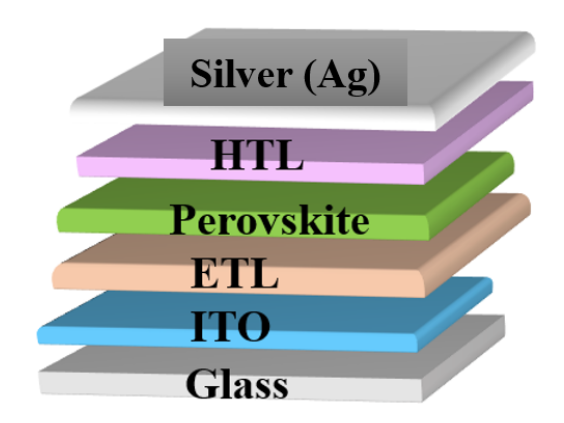


Figure 4.2: PSC architecture used in this study.

Electron transport layer (ETL) To deposit the ETL, a SnO₂ solution was prepared by diluting commercially available tin oxide colloidal dispersion (15% in H₂O, Alfa Aesar) with DI water in a 1:4 volume ratio [34]. The diluted SnO₂ solution was then spin-coated onto the ITO substrates immediately after the UV-ozone treatment. Spin-coating was performed at a rpm of 3000 for 30 seconds to ensure uniform film formation. Following deposition, the substrates were subjected to a thermal annealing step at 150°C for 30 minutes to promote adhesion and crystallization of the ETL layer. Both the preparation of the SnO₂ solution and the spin-coating process were conducted under ambient atmospheric conditions.

Hole transport layer (HTL) The HTL was deposited using Spiro-OMeTAD as the transport material. To prepare the HTL solution, 86 mg of Spiro-OMeTAD was mixed in 1 mL of chlorobenzene. To enhance the conductivity and stability of the layer, the following dopants were added to the solution:

- 20 μ L of LiTFSI from a 500 mg/mL stock solution in acetonitrile (ACN),
- 11 μ L of FK 209 (tris(2-(1H-pyrazol-1-yl)-4-tert-butylpyridine)cobalt(II) bis(hexafluorophosphate)) from a 300 mg/mL stock solution in ACN,
- 34 μ L of 4-tert-butylpyridine.

The resulting HTL solution was dynamically spin-coated onto the perovskite layer at 4000 rpm for 30 seconds to ensure uniform coverage.

After spin coating, the samples were stored overnight in a dry-air environment to allow for oxidation of the Spiro-OMeTAD, which is essential for achieving optimal hole transport properties [35].

Chagre Transport Layer Deposition The next day, the silver back contact was deposited using thermal evaporation to ensure a uniform and stable electrode layer. The deposition process was carried out in a Thermal vapor deposition unit at a controlled rate of 1 A per second, achieving a final thickness of approximately 80 nm. A conformal mask made of stainless steel with eight defined pixels (cells) was used during the evaporation process to pattern the electrode. Fig. 4.3 showing the thermal vapour deposition of silver. After the silver deposition was complete, the masks were carefully removed from the films, leaving behind well-defined contact areas.



Figure 4.3: Thermal vapour deposition of silver.

4.2 Device Fabrication of FAMA PSCs

Methodology for FAPbI₃ thin film deposition The perovskite absorber layer was deposited using a two-step spin-coating process. First, a precursor solution containing 1.5 M lead iodide was prepared in a solvent mixture of N,N-dimethylformamide (DMF) and dimethyl sulfoxide (DMSO) in a 9:1 volume ratio. This solution was spin-coated onto the ITO substrate at 1500 rpm for 30 seconds. The coated film was then annealed at 70°C for 1 minute and allowed to cool to room temperature.

In the second step, a mixed organic halide solution containing formamidinium iodide (FAI), methylammonium chloride (MACl), and methylammonium bromide (MABr) in a molar ratio of 90:9:9 was prepared in tertbutyl alcohol (TBA). This solution was dynamically spin-coated over the pre-deposited PbI₂ layer at 2000 rpm for 30 seconds.

Following deposition, the films were subjected to thermal annealing at 150°C for 15 minutes under inert conditions inside a nitrogen-filled glove box. This thermal treatment facilitated the complete conversion of precursors into a uniform and crystalline FAPbI₃ perovskite phase.

Device Fabrication The device fabrication in this study was based on the planar n-i-p architecture. All layers were deposited via spin coating, with careful control over environmental conditions to ensure high-quality film formation and device performance.

The SnO_2 electron transport layer was deposited under ambient atmospheric conditions. Additionally, the second-step spin-coating process where a solution of FAI:MACl:MABr (90:9:9) in tert-butyl alcohol was applied, was also performed in ambient air.

All other deposition steps, including the PbI₂ layer, Spiro-OMeTAD hole transport layer, and the final silver electrode, were carried out under an inert nitrogen atmosphere inside a glove box. This controlled environment minimized moisture and oxygen exposure, which is important for the stability and reproducibility of perovskite solar cells. Fig. 4.4 shows the complete device fabrication process for FAMA PSCs.

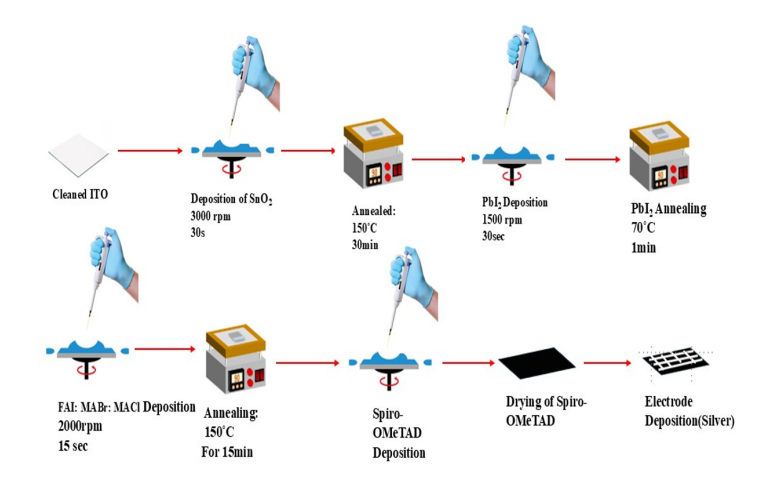


Figure 4.4: Preparation Method for FAMA-Based Perovskite Solar Cells

4.3 Device Fabrication of Triple Cation Perovskite

For the active perovskite layer, a triple-cation perovskite composition with the formula $Cs_{0.05}FA_{0.81}MA_{0.14}PbI_{2.55}Br_{0.45}$ was employed. The perovskite precursor solution was prepared 1.2 M using a solvent mixture of DMF and DMSO.

Cesium incorporation was achieved by first preparing a 1.5 M CsI stock solution in DMSO. A precise volume of this CsI solution was added to

the perovskite precursor. The complete preparation and processing were conducted inside a nitrogen-filled glove box.

Prior to perovskite deposition, the electron transport layer (ETL)-coated substrates underwent UV-ozone treatment for 30 minutes to improve surface wettability and film uniformity.

The perovskite film was deposited using a two-step spin-coating process:

- Step 1: 2000 rpm for 10 seconds
- Step 2: 3000 rpm for 20 seconds

During the second spin step, 60 μ L of chlorobenzene was dynamically dispensed onto the substrate 5 seconds before the end of the spin cycle. This antisolvent step was critical for improving crystallinity and achieving uniform film morphology.

Immediately after spin coating, the films exhibited a characteristic black color, indicating successful crystallization of the perovskite phase. The films were then annealed at 100°C for 15 minutes to further enhance crystal growth. Both the spin-coating and annealing steps were performed entirely within the glove box to ensure a controlled atmosphere.

Subsequent to perovskite deposition, the hole transport layer (Spiro-OMeTAD) was applied, followed by thermal evaporation of silver (Ag) to complete the device structure. The complete device fabrication process of Triple cation perovskite is shown in the fig. 4.5

4.4 Incorporating Ionic Liquids for Interface Engineering in PSCs

All fabrication steps were identical to those used for FAMA perovskite solar cells. However, to modify the crystallization behavior, 1 mol% of formamidinium acetate (FAAc) relative to PbI_2 was added to the PbI_2 precursor solution. Fig. 4.6 shows the complete fabrication process of FAAc modified PSCs.

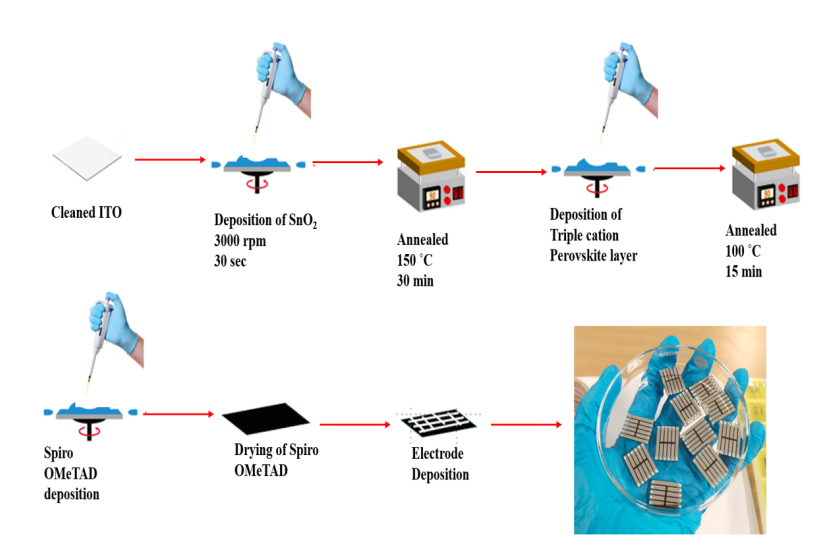


Figure 4.5: Preparation Method for triple cation PSCs.

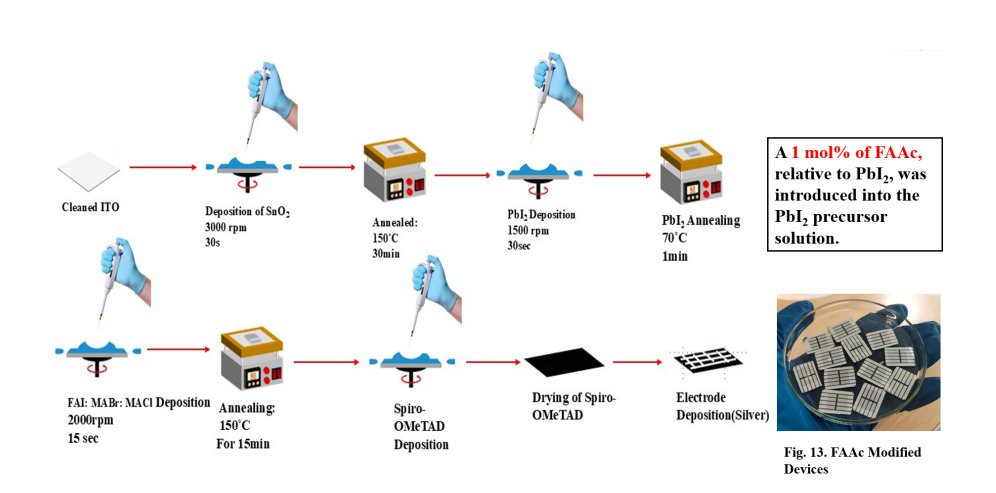


Figure 4.6: Preparation Method for FAAc modified Perovskite Solar Cells.

Chapter 5

Experimental Results and Interpretation

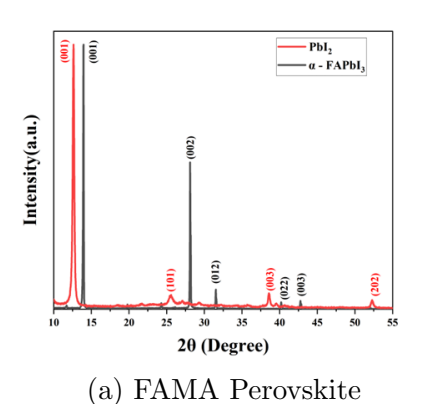
This part provides an in-depth discussion of the experimental results obtained from all the fabricated PSCs devices. It encompasses a thorough analysis of their structural, optical, morphological, and PV properties. The insights gained from these evaluations help in understanding the factors influencing device efficiency and reliability, thereby guiding further improvements in materials selection and fabrication techniques.

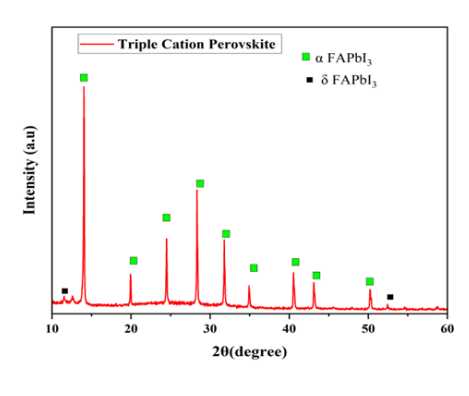
5.1 X-Ray Diffraction (XRD) : Revealing Crystal Structures

XRD is a powerful and widely adopted technique to investigate the crystal structure of perovskite films. It provides valuable information about crystalline phases, preferred orientations, lattice parameters, and the presence of secondary phases or impurities.

In this analysis, a diffractometer equipped with a Cu K α radiation source ($\lambda=1.5406\,\text{Å}$) was used. The system includes a sample holder and a detector that records the intensity of diffracted X-rays. The diffraction patterns were collected across a 2θ range of 10° to 55° , enabling comprehensive structural characterization.

The normalized XRD patterns of the FAMA and Triple Cation perovskite films are presented in Fig. 5.1a and Fig. 5.1b, respectively.





(b) Triple Cation Perovskite

Figure 5.1: Normalized XRD patterns of (a) FAMA and (b) Triple Cation perovskite films.

In Fig. 5.1a, the XRD pattern of the FAMA perovskite shows distinct diffraction peaks at 14.1°, 28.4°, and 31.8°, corresponding to the (001), (002), and (012) planes of the α -FAPbI₃ phase. A small peak near 12.6° is attributed to unreacted PbI₂, indicating slight residual precursor, which can sometimes help in reducing interfacial defects.

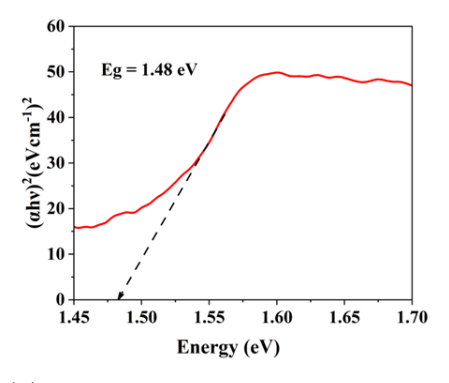
In contrast, Fig. 5.1b displays the XRD pattern for the Triple Cation perovskite film with composition $Cs_{0.05}FA_{0.81}MA_{0.14}PbI_{2.55}Br_{0.45}$. The peaks are sharper and more intense, reflecting a highly ordered crystalline structure. The addition of Cs^+ ions appears to suppress the formation of non-perovskite phases, with no significant peaks corresponding to the δ -phase, indicating improved phase stability.

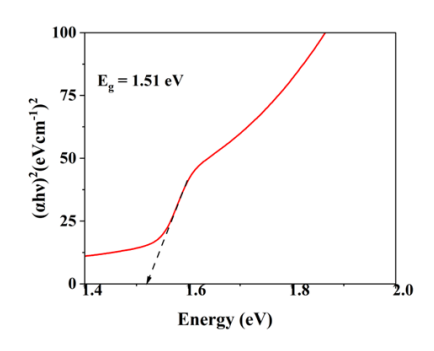
These observations suggest that the Triple Cation composition leads to better structural properties and stability, which are essential for efficient and durable perovskite solar cell performance.

5.2 UV-Vis Spectroscopy: A Tool for Bandgap Analysis

UV-Visible spectroscopy is a fundamental technique for studying how materials interact with ultraviolet and visible light. It provides significant understanding of their optical and electronic characteristics through measuring light absorption, transmission, and reflection. One of the most important applications of UV-Visible spectroscopy is determining the band gap, a key property that defines the energy levels of material and its ability to absorb light efficiently. The Tauc plots presented in fig. 5.2a and fig.

5.2b correspond to the FAMA and triple-cation perovskite films, respectively, highlighting their distinct optical bandgaps.





- (a) Tauc plot for FAMA perovskite.
- (b) Tauc plot for triple cation perovskite.

Figure 5.2: Optical bandgap determination using Tauc plots for (a) FAMA and (b) triple cation perovskite films.

The optical bandgap energies of the FAMA and triple-cation perovskite thin films were determined using Tauc plots, which are widely applied for analyzing the bandgap of direct bandgap semiconductors. The Tauc relation,

$$(\alpha h\nu)^2 = A(h\nu - E_q),$$

where α is the absorption coefficient, $h\nu$ is the photon energy, and E_g is the optical bandgap, was used to estimate the values. As shown in Fig. 5.2a, the extrapolation of the linear region of the $(\alpha h\nu)^2$ versus $h\nu$ plot for the FAMA film intersects the energy axis at approximately 1.48 eV, indicating its optical bandgap.

Similarly, for the triple-cation perovskite film, the Tauc plot shown in Fig. 5.2b reveals a slightly higher bandgap of about 1.51 eV. The incorporation of Cs⁺ ions in the triple-cation structure is known to slightly modify the lattice and electronic properties, leading to a small bandgap widening. These bandgap values are optimal for single-junction photovoltaic applications, offering efficient sunlight absorption while minimizing thermalization losses. The slight variation in bandgap also reflects the tunability of the perovskite material system through compositional engineering.

5.3 Scanning Electron Microscopy (SEM):

SEM plays a vital role in characterizing the surface morphology and microstructural features of perovskite films. This high-resolution imaging technique enables detailed visualization of surface texture, grain boundaries, and crystallinity at the micro and nanoscale, making it indispensable for evaluating the quality of perovskite absorber layers, key determinants of SC performance.

SEM was employed to examine the surface morphology of FAMA and triple-cation perovskite films. The captured images were analyzed using ImageJ software to estimate the grain sizes by measuring individual grain dimensions across various regions of each film. Subsequently, the grain size data were plotted into histograms using Origin software, providing a clear statistical representation of the grain size distribution and morphological variations between the two compositions.

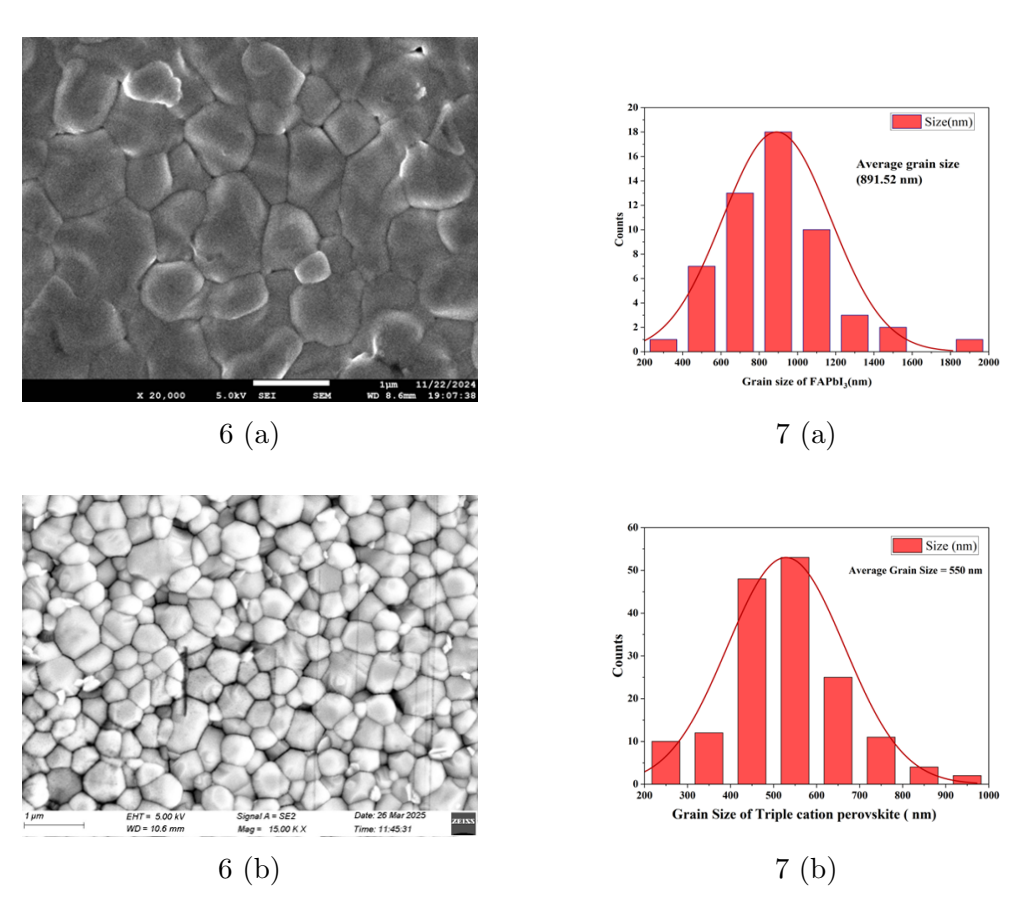


Figure 5.3: (6) SEM images and (7) grain size distributions for (a) FAPbI₃ and (b) triple-cation perovskite films.

As shown in Figure 5.3, the FAMA film exhibits a broad grain size distribution, with an average grain size of approximately 891.52 nm. The histogram reveals a Gaussian-like distribution, indicative of uniform grain growth with instances of grain coalescence. Larger grains generally suggest fewer grain boundaries, which serve as charge carrier recombination centers. Their reduction facilitates improved charge transport and overall device efficiency.

Conversely, Figure 5.3 shows the grain size distribution of the triplecation perovskite film, revealing a smaller average grain size of around 550 nm. The distribution is more symmetric and compact, reflecting a more uniform crystallization process. This refinement is attributed to the incorporation of Cs⁺ and MA⁺ in the perovskite composition, which is known to influence nucleation and growth dynamics during film formation.

Grain size impacts the PV performance of perovskite solar cells. Larger grains help suppress non-radiative recombination by reducing the number of grain boundaries, thereby enhancing the efficiency of charge collection. On the other hand, smaller, uniformly distributed grains while offering slightly higher boundary density can improve film uniformity and mechanical stability.

Therefore, SEM-based grain size analysis is not merely a visualization technique, but a critical diagnostic tool for correlating the morphological quality of perovskite films with their electronic behavior and photovoltaic performance.

5.4 J-V Testing for Device Performance

The perovskite solar cell (PSC) architecture with the configuration ITO/SnO_2 /Perovskite /Spiro/Ag was successfully fabricated using well established experimental procedures. To evaluate their performance, the fabricated cells were subjected to testing under a solar simulator, simulating standard sunlight conditions. This testing provided critical insights into the cells light responsiveness and overall efficiency, ensuring their suitability for photovoltaic applications.

5.4.1 Solar Simulator

A solar simulator is an essential instrument for testing and characterizing solar cells, including perovskite-based devices. It accurately mimics natural sunlight to evaluate the electrical performance of SCs under controlled laboratory conditions. In this study, the solar simulator was calibrated to

produce the AM1.5G spectrum, which closely resembles the solar irradiance received on Earth's surface. The light intensity was adjusted using a calibrated fluxmeter to replicate standard illumination conditions (1 sun, i.e., 100 mW/cm²) as shown in Fig. 5.4 6 (a).

From the J–V measurements, several key PV parameters were extracted:

Short-circuit current density (J_{sc}) : Defined as the current per unit area when the voltage across the cell is zero. It indicates the peak photocurrent the device can generate and is calculated as:

$$J_{sc} = \frac{I_{sc}}{A}$$

where A is the active area of the SC.

Fill Factor (FF): This parameter measures how square the J–V curve is. It is the ratio of the maximum power output $(V_{mp} \times J_{mp})$ to the product of open-circuit voltage and short-circuit current density:

$$FF = \frac{V_{mp} \times J_{mp}}{V_{oc} \times J_{sc}}$$

Power Conversion Efficiency (PCE): A key performance indicator showing how efficiently the SC converts sunlight into electricity. It is given by the ratio of electrical power output to the input solar power:

$$PCE = \frac{V_{oc} \times J_{sc} \times FF}{P_{in}} \times 100\%$$

where P_{in} is the incident light power density, usually 100 mW/cm² under standard testing conditions (1 sun).

These parameters provide a comprehensive assessment of solar cell performance and are crucial for evaluating and optimizing the design of perovskite solar cells.

5.4.2 J-V Measurmnet

J-V measurements are one of the most fundamental and informative techniques for characterizing PV devices, including PSCs. This provides direct insights into the electrical behavior and performance of the solar cell under illumination. In particular, it enables the extraction of key PV parameters such as $J_{\rm sc}$), $V_{\rm oc}$, FF, and PCE. These metrics help evaluate device quality, identify loss mechanisms, and compare the impact of different material compositions and processing strategies.

The J–V characteristics were obtained under simulated AM1.5G illumination using the Ossila Solar Cell I–V Test System. Forward and reverse scans were performed between -0.1 V and 1.1 V. The resulting curves are shown in Fig. 5.4, while the extracted parameters are summarized in table 5.1.

Table 5.1: PV performance parameters of FAMA and triple cation-based PSCs

Perovskite Composition	Scan Direction	$J_{\rm sc}~({ m mA/cm^2})$	FF (%)	V _{oc} (V)	PCE (%)
FAMA	Reverse	20.64	68.64	0.96	13.33
FAMA	Forward	19.83	53.29	0.89	9.40
Triple cation	Reverse	22.21	75.53	1.04	17.46
Triple cation	Forward	21.97	59.03	1.03	13.37

Table 5.2: PV parameters of control and FAAc (1%) treated devices.

Sample	Scan Direction	$J_{\rm sc}~({ m mA/cm^2})$	FF (%)	$V_{oc}(V)$	PCE (%)
Control	Reverse	20.33	67.06	0.85	11.65
Control	Forward	20.33	65.39	0.82	10.94
FAAc-1%	Reverse	17.57	65.05	0.97	11.15
FAAc-1%	Forward	17.52	46.15	0.89	7.24

FAMA-Based Devices: Figure 5.4 shows clear hysteresis behavior, with the reverse scan yielding a significantly higher PCE (13.33%) than the forward scan (9.4%). The decrease in FF and $V_{\rm oc}$ in the forward scan indicates ionic migration and interfacial instability.

Triple-Cation Devices: As shown in Fig. 5.4, the triple-cation perovskite demonstrates improved performance with minimal hysteresis. The reverse scan yields a high PCE of 17.46%, and the forward scan maintains a decent 13.37%, signifying improved film morphology and energetic alignment due to compositional engineering.

FAAc Treatment: FAAc (1%) treatment enhances $V_{\rm oc}$ (up to 0.97 V) in the reverse scan, suggesting reduced defect-assisted recombination. However, the sharp FF drop (46.15%) in the forward scan (Figure 5.4) leads to a lower forward PCE (7.24%), implying possible adverse effects at the interface or increased ion migration due to additive incorporation.

Moreover, hysteresis behavior, deduced from forward and reverse scans, can reveal underlying phenomena such as ionic migration, interfacial traps, or capacitive effects.

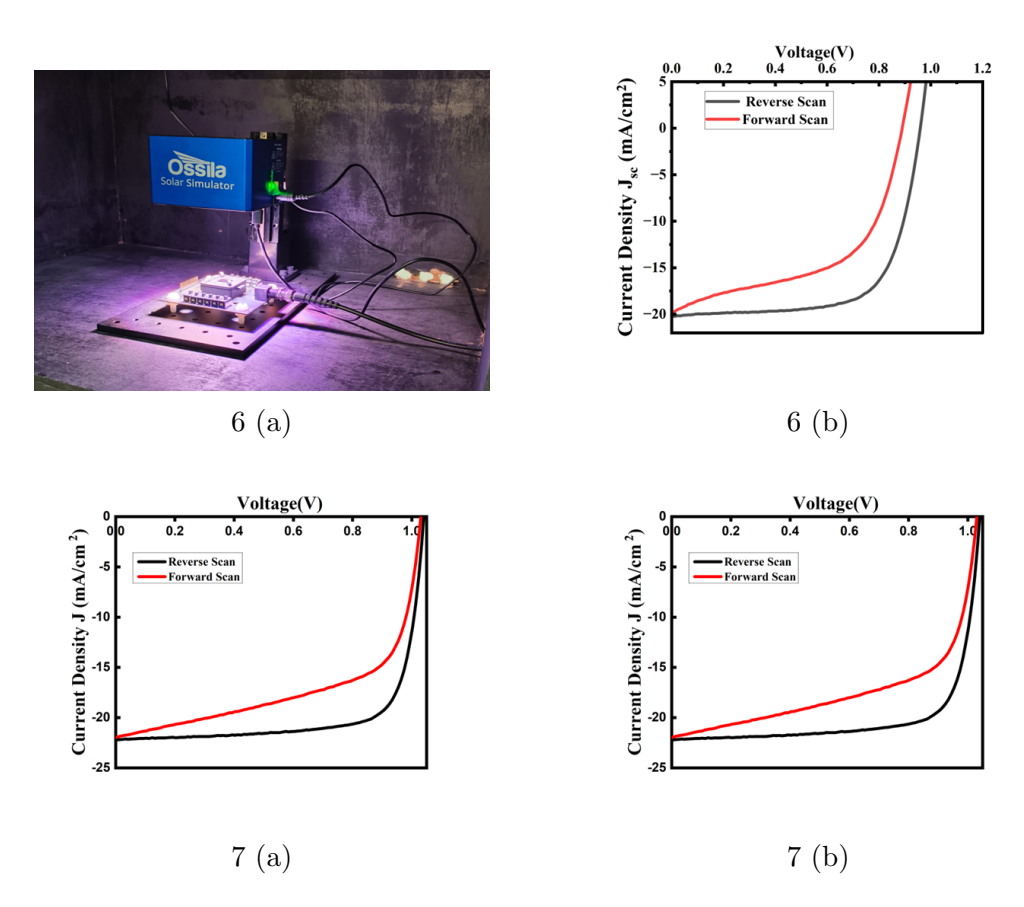
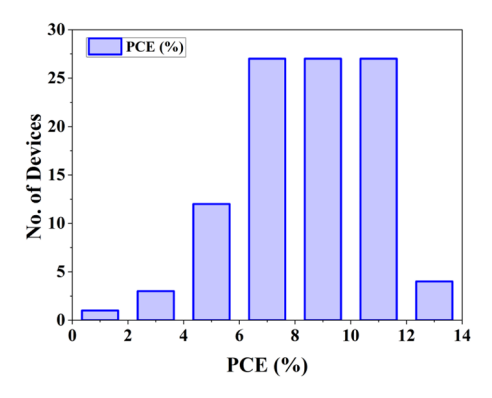
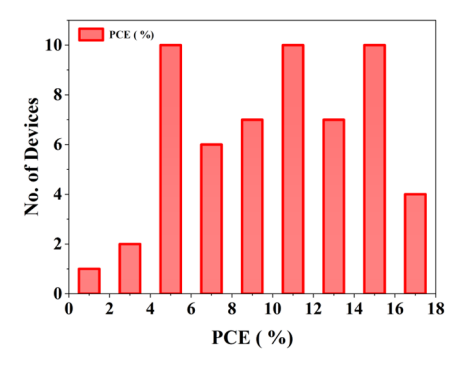


Figure 5.4: 6 (a) Solar Simulator, 6 (b)) J-V curve of the FAMA PSC, 7 (a) J-V curve of the Triple Cation PSC, 7 (b) J–V curves of the control and FAAc-modified PSCs.

5.5 PCE Distribution Analysis

To evaluate the statistical performance and reproducibility of the fabricated PSCs, histograms showing the distribution of PCE were analyzed for different compositions and processing conditions.





- (a) PCE Distribution FAMA PSCs.
- (b) PCE Distribution Triple cation perovskite solar cells.

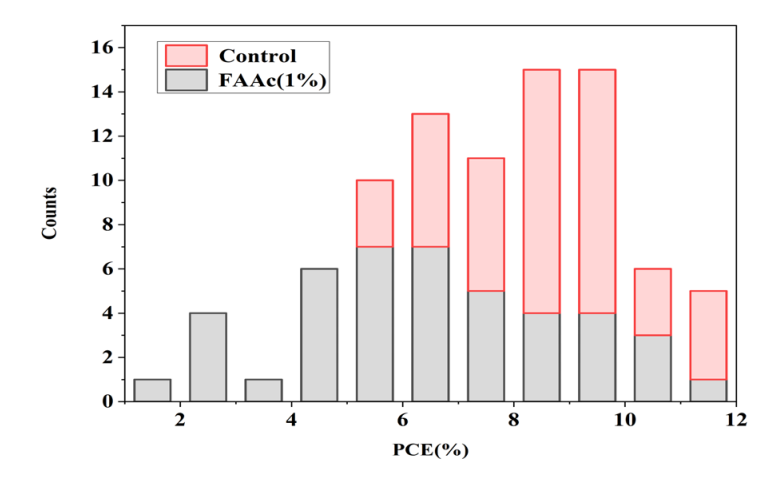


Figure 5.6: PCE distribution of control and FAAc modified perovskite solar cells

Fig. 5.5a displays the PCE distribution for FAMA-based perovskite solar cells. The histogram reveals that the majority of devices exhibited PCEs in the range of 6% to 10%, with a strong peak around 8–10%. Notably, over 25 devices demonstrated PCE values in this high-performing range,

suggesting a relatively good reproducibility and moderate performance for this composition.

In contrast, Fig. 5.5b presents the PCE distribution for triple-cation-based perovskite solar cells. The PCE values are more broadly distributed, spanning from 2% to 18%. Several devices reached PCEs above 14%, with three distinct peaks observed at 6%, 10%, and 14%, respectively. This wider distribution indicates greater variability in device performance but also demonstrates the potential for achieving higher efficiencies with triple-cation formulations compared to FAMA.

Furthermore, Fig. 5.6 compares the PCE distribution of control devices with those processed with 1% FAAc additive. The histogram clearly shows a shift toward higher efficiency in FAAc-treated devices. The control devices mainly peaked around 8–10%, while the FAAc group exhibited a broader and more balanced distribution, with a noticeable increase in device counts in the 6–9% range. The FAAc additive appears to improve not only the average PCE but also the uniformity of device performance, likely by enhancing film morphology and defect passivation.

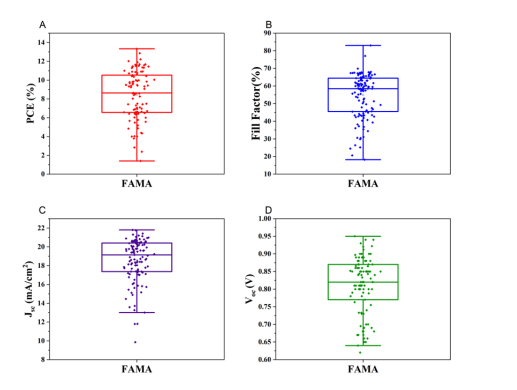
Overall, these PCE distribution analyses provide key insights into the impact of compositional engineering and additive processing on device efficiency and reproducibility.

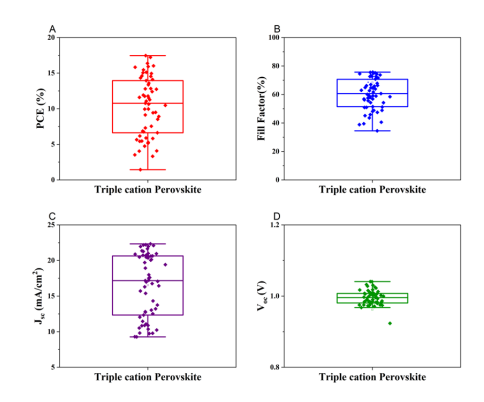
5.6 Statistical Analysis of Photovoltaic Parameters

To gain deeper insights into device performance and uniformity, box plots were generated to evaluate the distribution of key photovoltaic parameters, namely PCE, FF, J_{sc} , and V_{oc} for different device compositions and treatments.

Fig. 5.7a and fig. 5.7b compares the photovoltaic performance between FAMA and triple-cation-based perovskite devices. For PCE (panel A), the triple-cation devices exhibit a significantly higher median value and a narrower spread, indicating improved efficiency and better reproducibility. The fill factor (panel B) follows a similar trend, with triple-cation compositions achieving higher and more consistent FF values.

The J_{sc} (panel C) for triple-cation devices also shows an improvement, with both a higher median and reduced variation compared to FAMA. However, for V_{oc} (panel D), both systems show similar distributions, though the triple-cation devices display a slightly tighter range, reflecting enhanced uniformity.





- (a) Box plot comparison of key photovoltaic parameters for FAMA perovskite solar cells devices.
- (b) Box plot comparison of key photovoltaic parameters for triple cation perovskite solar cells devices.

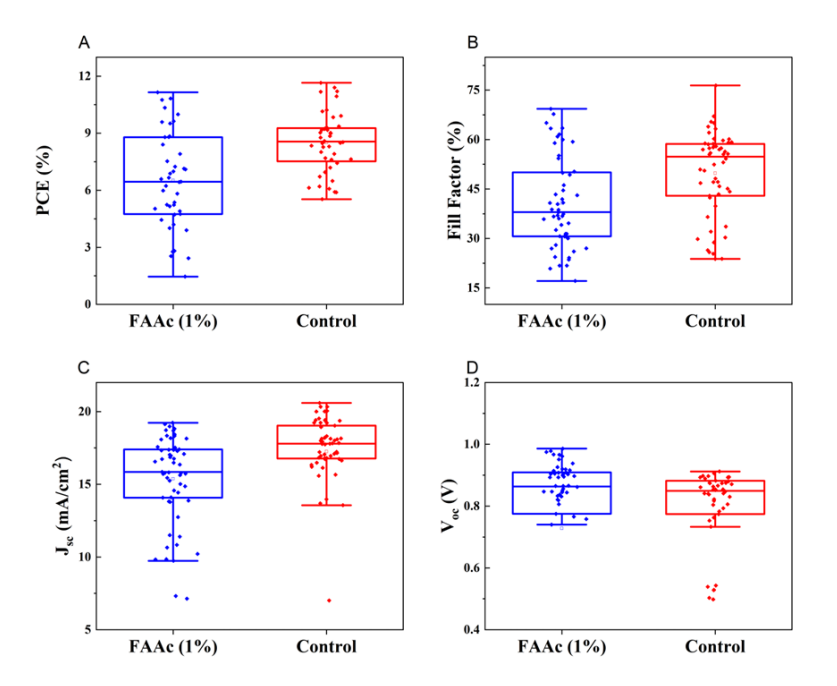


Figure 5.8: Box plot comparison of key photovoltaic parameters for FAAc modified perovskite solar cells devices.

Figure 5.8 compares the impact of FAAc (1%) additive treatment on device performance relative to untreated control devices. While the control devices generally exhibit higher median values for PCE, FF, and J_{sc} , the

FAAc-treated devices demonstrate a wider distribution. This indicates that although FAAc improves film formation, there may be batch-to-batch variability or incomplete optimization at the tested concentration.

Interestingly, the V_{oc} (panel D) shows a higher average in FAAc-treated devices, suggesting potential benefits in defect passivation and improved charge carrier lifetimes. The broader data range in some parameters also suggests ongoing optimization is necessary to fully harness the benefits of FAAc incorporation.

Overall, these box plot analyses highlight the superior reproducibility and performance of triple-cation devices and the potential of FAAc as a performance-tuning additive in FAMA-based perovskites.

Chapter 6

Conclusion

This thesis demonstrates a comprehensive understanding of compositional engineering in perovskite precursors aimed at stabilizing the photoactive α -phase. Initially, two types of PSCs, FAMA and triple-cation, were fabricated. The PV performance of these devices yielded PCEs of 17.46% and 13.33%, with FF of 68% and 75%, V_{OC} of 0.96 V and 1.04 V, and J_{SC} of 20.64 mA/cm² and 22.21 mA/cm², respectively.

These results highlighted critical factors influencing device performance, such as compositional tuning, crystallinity, and defect passivation.

To further explore defect mitigation and enhance device stability, the thesis investigates the addition of the ionic liquid formamidine acetate (FAAc) into the PbI₂ precursor. A 1 mol% of FAAc, relative to PbI₂, was introduced into the PbI₂ precursor solution. This modification led to a notable enhancement in the $V_{\rm OC}$, indicating effective defect passivation. The modified device exhibited a PCE of 11.15%, with a $V_{\rm OC}$ of 0.89 V, $J_{\rm SC}$ of 17.57 mA/cm², and FF of 65.05%.

Overall, this work underscores the need for a holistic approach to optimize precursor composition, enhance phase stability, and minimize defect states. The findings from this research offer a solid basis for advancing interface and composition engineering in future perovskite solar cell technologies.

Bibliography

- [1] Ho Soonmin, Hardani, Pronoy Nandi, Benard Samwel Mwankemwa, Thembinkosi Donald Malevu, and Muhammad Imran Malik. Overview on different types of solar cells: An update. *Applied Sciences*, 13(4), 2023.
- [2] Ajay Kumar Jena, Ashish Kulkarni, and Tsutomu Miyasaka. Halide perovskite photovoltaics: Background, status, and future prospects. *Chemical Reviews*, 119(5):3036–3103, 2019.
- [3] Lukas Schmidt-Mende, Vladimir Dyakonov, Selina Olthof, Feray Ünlü, Khan Lê, Dr. Sanjay Mathur, Andrei Karabanov, Doru Lupascu, Laura Herz, Alexander Hinderhofer, Frank Schreiber, Alexey Chernikov, David Egger, Oleksandra Shargaieva, Caterina Cocchi, Eva Unger, Michael Saliba, Mahdi Malekshahi, Martin Kroll, and Claudia Draxl. Roadmap on organic-inorganic hybrid perovskite semiconductors and devices. *APL Materials*, 9:109202, 10 2021.
- [4] Chufeng Qiu, Yan Wu, Jiaxing Song, Wentao Wang, and Zaifang Li. Efficient planar perovskite solar cells with zno electron transport layer. *Coatings*, 12(12), 2022.
- [5] Alexandre Gheno, Sylvain Vedraine, Bernard Ratier, and Johann Bouclé. -conjugated materials as the hole-transporting layer in perovskite solar cells. *Metals*, 6(1), 2016.
- [6] Yonggui Sun, Ruiyuan Hu, Fei Wang, Taomiao Wang, Xiao Liang, Xianfang Zhou, Guo Yang, Yongjun Li, Fan Zhang, Quanyao Zhu, Xing'ao Li, and Hanlin Hu. Ionic liquid-regulated pbi2 layers and defect passivation for efficient perovskite solar cells. J. Mater. Chem. C, 12:5175–5183, 2024.
- [7] P C Choubey, A Oudhia, and R Dewangan. A review: Solar cell current scenario and future trends. *Recent Research in Science and Technology*, 4(8), Oct. 2012.

[8] L. Cutz, O. Masera, D. Santana, and A.P.C. Faaij. Switching to efficient technologies in traditional biomass intensive countries: The resultant change in emissions. *Energy*, 126:513–526, 2017.

[9]

- [10] Michael Saliba, Taisuke Matsui, Konrad Domanski, Ji-Youn Seo, Amita Ummadisingu, Shaik M. Zakeeruddin, Juan-Pablo Correa-Baena, Wolfgang R. Tress, Antonio Abate, Anders Hagfeldt, and Michael Grätzel. Incorporation of rubidium cations into perovskite solar cells improves photovoltaic performance. *Science*, 354(6309):206–209, 2016.
- [11] Dieter Weber. Ch3nh3pbx3, ein pb(ii)-system mit kubischer perowskitstruktur / ch3nh3pbx3, a pb(ii)-system with cubic perovskite structure. Zeitschrift für Naturforschung B, 33(12):1443–1445, 1978.
- [12] V. M. Goldschmidt. Krystallbau und chemische zusammensetzung. Berichte der deutschen chemischen Gesellschaft (A and B Series), 60(5):1263–1296, 1927.
- [13] Chonghea Li, Xionggang Lu, Weizhong Ding, Liming Feng, Yonghui Gao, and Ziming Guo. Formability of ABX_3 (X = F, Cl, Br, I) halide perovskites. Acta Crystallographica Section B, 64(6):702–707, Dec 2008.
- [14] Quinten A. Akkerman and Liberato Manna. What defines a halide perovskite? ACS Energy Letters, 5(2):604–610, 2020. PMID: 33344766.
- [15] Qi Chen, Nicholas De Marco, Yang (Michael) Yang, Tze-Bin Song, Chun-Chao Chen, Hongxiang Zhao, Ziruo Hong, Huanping Zhou, and Yang Yang. Under the spotlight: The organic–inorganic hybrid halide perovskite for optoelectronic applications. *Nano Today*, 10(3):355–396, 2015.
- [16] Samuel D. Stranks, Giles E. Eperon, Giulia Grancini, Christopher Menelaou, Marcelo J. P. Alcocer, Tomas Leijtens, Laura M. Herz, Annamaria Petrozza, and Henry J. Snaith. Electron-hole diffusion lengths exceeding 1 micrometer in an organometal trihalide perovskite absorber. *Science*, 342(6156):341–344, 2013.
- [17] Qingfeng Dong, Yanjun Fang, Yuchuan Shao, Padhraic Mulligan, Jie Qiu, Lei Cao, and Jinsong Huang. Electronhole diffusion lengths > 175 μm in solution-grown

- chįsub3į/su
- [18] Hye Ryung Byun, Dae Young Park, Hye Min Oh, Gon Namkoong, and Mun Seok Jeong. Light soaking phenomena in organic—inorganic mixed halide perovskite single crystals. *ACS Photonics*, 4(11):2813–2820, 2017.
- [19] Jin Young Kim, Jin-Wook Lee, Hyun Suk Jung, Hyunjung Shin, and Nam-Gyu Park. High-efficiency perovskite solar cells. *Chemical Reviews*, 120(15):7867–7918, 2020. PMID: 32786671.
- [20] Tai Wu, Dongyang Zhang, Yangmei Ou, Huili Ma, Anxin Sun, Rongmei Zhao, Liqiong Zhu, Runtao Wang, Rongshan Zhuang, Gaoyuan Liu, Yuanju Zhao, Qian Lai, and Yong Hua. Efficient perovskite solar cells enabled by large dimensional structured hole transporting materials. J. Mater. Chem. A, 9:1663–1668, 2021.
- [21] Faiza Jan Iftikhar, Qamar Wali, Shengyuan Yang, Yaseen Iqbal, Rajan Jose, Shamsa Munir, Irfan A. Gondal, and Muhammad Ejaz Khan. Structural and optoelectronic properties of hybrid halide perovskites for solar cells. Organic Electronics, 91:106077, 2021.
- [22] Tejas S. Sherkar, Cristina Momblona, Lidón Gil-Escrig, Jorge Ávila, Michele Sessolo, Henk J. Bolink, and L. Jan Anton Koster. Recombination in perovskite solar cells: Significance of grain boundaries, interface traps, and defect ions. ACS Energy Letters, 2(5):1214–1222, 2017. PMID: 28540366.
- [23] Sheng Zou, Suxia Liang, Tianyu Yu, Jie Su, Yunlei Jiang, Renjie Hua, Zhiyuan Huang, Wenjun Zhang, Lei Shi, Yukun Guo, Qingshun Dong, Yaling Han, Hongru Ma, Yilin Gao, Yantao Shi, and Yuan Dong. Scalable large area perovskite solar cell modules fabricated with high humidity tolerance by vacuum deposition. *Materials Today Energy*, 40:101506, 2024.
- [24] Corinna Ponti, Giuseppe Nasti, Diego Di Girolamo, Irene Cantone, Fahad A. Alharthi, and Antonio Abate. Environmental lead exposure from halide perovskites in solar cells. *Trends in Ecology Evolution*, 37(4):281–283, 2022.
- [25] Neetika Yadav and Ayush Khare. Resolving interfacial challenges in perovskite solar cells: From defect control to energy band optimization. Surfaces and Interfaces, 56:105593, 2025.

- [26] Filippo De Angelis, Daniele Meggiolaro, Edoardo Mosconi, Annamaria Petrozza, Mohammad Khaja Nazeeruddin, and Henry J. Snaith. Trends in perovskite solar cells and optoelectronics: Status of research and applications from the psco conference. *ACS Energy Letters*, 2(4):857–861, 2017.
- [27] Jin Cui, Huailiang Yuan, Junpeng Li, Xiaobao Xu, Yan Shen, Hong Lin, and Mingkui Wang and. Recent progress in efficient hybrid lead halide perovskite solar cells. Science and Technology of Advanced Materials, 16(3):036004, 2015. PMID: 27877815.
- [28] Giles E. Eperon, Samuel D. Stranks, Christopher Menelaou, Michael B. Johnston, Laura M. Herz, and Henry J. Snaith. Formamidinium lead trihalide: a broadly tunable perovskite for efficient planar heterojunction solar cells. *Energy Environ. Sci.*, 7:982–988, 2014.
- [29] Shuping Pang, Hao Hu, Jiliang Zhang, Siliu Lv, Yaming Yu, Feng Wei, Tianshi Qin, Hongxia Xu, Zhihong Liu, and Guanglei Cui. Nh2chnh2pbi3: An alternative organolead iodide perovskite sensitizer for mesoscopic solar cells. *Chemistry of Materials*, 26(3):1485–1491, 2014.
- [30] Xueping Liu, Deying Luo, Zheng-Hong Lu, Jae Sung Yun, Michael Saliba, Sang Il Seok, and Wei Zhang. Stabilization of photoactive phases for perovskite photovoltaics. *Nature reviews. Chemistry*, 7(7):462—479, July 2023.
- [31] Zhen Li, Mengjin Yang, Ji-Sang Park, Su-Huai Wei, Joseph J. Berry, and Kai Zhu. Stabilizing perovskite structures by tuning tolerance factor: Formation of formamidinium and cesium lead iodide solid-state alloys. *Chemistry of Materials*, 28(1):284–292, 2016.
- [32] Andreas Binek, Fabian C. Hanusch, Pablo Docampo, and Thomas Bein. Stabilization of the trigonal high-temperature phase of formamidinium lead iodide. *The Journal of Physical Chemistry Letters*, 6(7):1249–1253, 2015. PMID: 26262982.
- [33] Michael Saliba, Juan-Pablo Correa-Baena, Christian M. Wolff, Martin Stolterfoht, Nga Phung, Steve Albrecht, Dieter Neher, and Antonio Abate. How to make over 20% efficient perovskite solar cells in regular (n–i–p) and inverted (p–i–n) architectures. *Chemistry of Materials*, 30(13):4193–4201, 2018.

- [34] Ying-Han Liao, Yin-Hsuan Chang, Ting-Han Lin, Kun-Mu Lee, and Ming-Chung Wu. Recent advances in metal oxide electron transport layers for enhancing the performance of perovskite solar cells. *Materials*, 17(11), 2024.
- [35] Onkar S. Game, Joel A. Smith, Tarek I. Alanazi, Michael Wong-Stringer, Vikas Kumar, Cornelia Rodenburg, Nick J. Terrill, and David G. Lidzey. Solvent vapour annealing of methylammonium lead halide perovskite: what's the catch? *J. Mater. Chem. A*, 8:10943–10956, 2020.